J|A|C|S ARTICLES

Published on Web 01/08/2009

Kinetic Analysis of β-Phosphoglucomutase and Its Inhibition by Magnesium Fluoride

Marko Goličnik,[†,⊥] Luis F. Olguin,[†] Guoqiang Feng,[‡] Nicola J. Baxter,[§] Jonathan P. Waltho,[§,||] Nicholas H. Williams,*[,‡] and Florian Hollfelder*[,†]

Department of Biochemistry, University of Cambridge, Cambridge CB2 1GA, United Kingdom, Centre for Chemical Biology, Department of Chemistry, University of Sheffield, Sheffield S3 7HF, United Kingdom, Department of Molecular Biology & Biotechnology, University of Sheffield, Sheffield S10 2TN, United Kingdom, and Faculty of Life Sciences and Manchester Interdisciplinary Biocentre, The University of Manchester, Manchester M1 7DN, United Kingdom

Received August 13, 2008; E-mail: fh111@cam.ac.uk; n.h.williams@sheffield.ac.uk

Abstract: The isomerization of β-glucose-1-phosphate (βG1P) to β-glucose-6-phosphate (G6P) catalyzed by β-phosphoglucomutase (βPGM) has been examined using steady- and presteady-state kinetic analysis. In the presence of low concentrations of β-glucose-1,6-bisphosphate (βG16BP), the reaction proceeds through a Ping Pong Bi Bi mechanism with substrate inhibition ($k_{cat} = 65\ s^{-1}$, $K_{\beta G1P} = 15\ \mu M$, $K_{\beta G16BP} = 0.7\ \mu M$, $K_i = 122\ \mu M$). If αG16BP is used as a cofactor, more complex kinetic behavior is observed, but the nonlinear progress curves can be fit to reveal further catalytic parameters ($k_{cat} = 74\ s^{-1}$, $K_{\beta G1P} = 15\ \mu M$, $K_{\beta G16BP} = 0.8\ \mu M$, $K_i = 122\ \mu M$, $K_{\alpha G16BP} = 91\ \mu M$ for productive binding, $K_{\alpha G16BP} = 21\ \mu M$ for unproductive binding). These data reveal that variations in the substrate structure affect transition-state affinity (approximately 140 000-fold in terms of rate acceleration) substantially more than ground-state binding (110-fold in terms of binding affinity). When fluoride and magnesium ions are present, time-dependent inhibition of the βPGM is observed. The concentration dependence of the parameters obtained from fitting these progress curves shows that a $\beta G1P \cdot MgF_3^- \cdot \beta PGM$ inhibitory complex is formed under the reaction conditions. The overall stability constant for this complex is approximately $2 \times 10^{-16}\ M^5$ and suggests an affinity of the MgF_3^- moiety to this transition-state analogue (TSA) of ≤70 nM. The detailed kinetic analysis shows how a special type of TSA that does not exist in solution is assembled in the active site of an enzyme. Further experiments show that under the conditions of previous structural studies, phosphorylated glucose only persists when bound to the enzyme as the TSA. The preference for TSA formation when fluoride is present, and the hydrolysis of substrates when it is not, rules out the formation of a stable pentavalent phosphorane intermediate in the active site of βPGM.

Introduction

To obtain a comprehensive and quantitative understanding of enzyme catalysis, the interactions of an enzyme active site with its substrate as it passes through its transition state (TS) need to be defined. The very short lifetime of the TS is currently well below the time scale of crystallographic analysis, so the structure of the enzyme−TS complex is not amenable to direct study by this method. Similar problems apply to the study of high-energy metastable intermediates that are closely related to the TS. Hence, the use of long-lived transition-state analogues (TSAs) has been an important element in deriving data from structural studies of enzymes that give insight into the precise alignment of functional groups and possible conformational changes of the surrounding protein that are important for catalytic activity. This is true for all enzymes, but especially important for very efficient enzymes, where multiple simultaneous interactions with the TS are likely to be required to provide sufficient catalytic power. Many of the biochemical reactions essential for life proceed extremely slowly in neutral aqueous solution at ambient temperature. Consequently, the enzymes that catalyze these reactions have to be remarkably efficient to reduce their half-lives to a viable time scale.[1,4] An important example is phosphate transfer, one of the central processes in biological chemistry, which is accelerated by factors up to 10^{21}, rendering the catalysts involved the most proficient enzymes known today.[2,3] If the reaction mechanism parallels that observed in solution, this means that they need to stabilize the very high-energy TSs of these reactions with extraordinary efficiency.[4]

[†] University of Cambridge.
[‡] Department of Chemistry, University of Sheffield.
[§] Department of Molecular Biology & Biotechnology, University of Sheffield.
[||] The University of Manchester.
[⊥] Permanent address: Institute of Biochemistry, Faculty of Medicine, University of Ljubljana, 1000 Ljubljana, Slovenia.

(1) Radzicka, A.; Wolfenden, R. *Science* **1995**, *267*, 90–3.
(2) Lad, C.; Williams, N. H.; Wolfenden, R. *Proc. Natl. Acad. Sci. U.S.A.* **2003**, *100*, 5607–10.
(3) Schroeder, G. K.; Lad, C.; Wyman, P.; Williams, N. H.; Wolfenden, R. *Proc. Natl. Acad. Sci. U.S.A.* **2006**, *103*, 4052–5.
(4) Wolfenden, R. *Chem. Rev.* **2006**, *106*, 3379–96.

Scheme 1. Reactions Catalyzed by βPGM Together with the Transition-State Analogue Formed in the Presence of Fluoride[a]

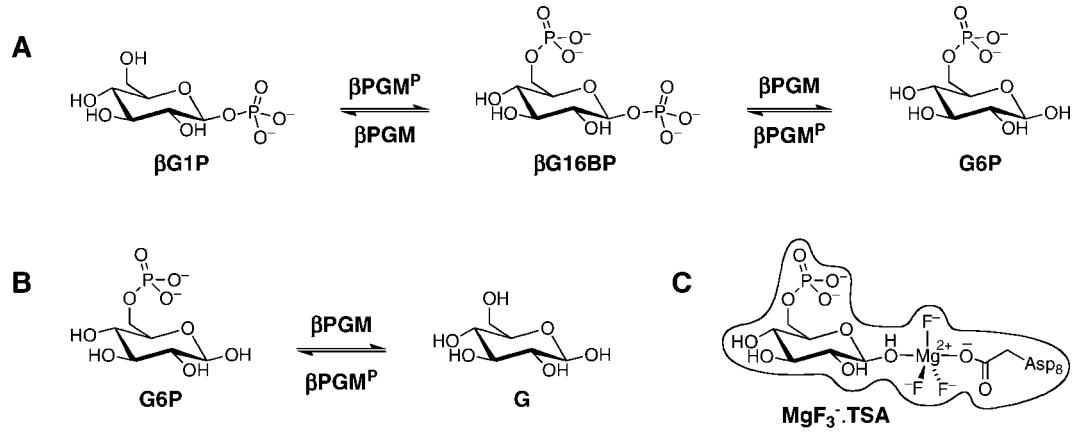

[a] (A) The mutase activity of βPGM catalyzes the transfer of phosphate between the 1 and 6 positions of glucose. (B) βPGM also catalyzes the hydrolysis of β-glucose-6-phosphate (G6P), the major species under equilibrium conditions, yielding glucose. (C) MgF_3^- combines with G6P in the active site to form a transition-state analogue for the phosphoryl transfer step (MgF_3^-•TSA).

β-phosphoglucomutase from *Lactococcus lactis* (βPGM, EC 5.4.2.6) is an example of one such enzyme and catalyzes the isomerization between β-glucose-1-phosphate (βG1P) and β-glucose-6-phosphate (G6P), using a magnesium(II) ion as a cofactor. The equilibrium lies strongly toward G6P ($K_{eq} = 28$ or $K_{eq} = 25$),[5,6] and the reaction proceeds through a ping-pong mechanism involving aspartyl-phosphoenzyme (βPGM^P) and β-glucose-1,6-bisphosphate (βG16BP) intermediates (Scheme 1A).[7] The report that βPGM could trap a phosphorane intermediate on this pathway to form a stable complex, which was characterized crystallographically,[8] strongly challenged the perception that phosphoranes derived from phosphate monoesters are not on the reaction pathway, as they are thought to be too unstable to exist. As well as the implications on the mechanism of this process, the structure was also significant in representing a true high-energy species on the reaction profile, directly providing information on how it interacts with the protein. However, the structural assignment was queried,[9] with the suggestion that the species in the active site was a TSA based on a metal fluoride complex (MgF_3^-) rather than a phosphorane (Scheme 1C).[10]

Several related metal fluoride complexes have been used as analogues for scissile phosphate groups[11−24] and currently provide the best available approximations of the TS for phosphoryl transferases. As beryllium prefers a tetrahedral geometry, BeF_3^- provides a stable mimic for reactive intermediates such as acyl phosphates.[16,25,26] Aluminum prefers an octahedral geometry,[27] which means that a nucleophile and leaving group can occupy axial positions, leaving AlF_4^- to take the place of the transferring PO_3^- moiety, so that derivatives can be considered TSAs in terms of charge, albeit not precisely in terms of steric demands.[28−31] However, trigonal-bipyramidal aluminum complexes containing a central AlF_3 have also been reported; these have a closer geometrical approximation to the phosphoryl moiety.[21,23,32] It has been suggested that the pH may influence whether an AlF_4^- or AlF_3 species forms in the enzyme active site,[21] although the reliability of the assignment of the AlF_3 species concerned has been questioned.[33,34] More recently, there have been reports of MgF_x^- complexes as an additional class of metal fluoride-based TSA−enzyme complexes in further structural studies, either as MgF_3^- [35−37] or as MgF_4^{2-} com-

(5) Marechal, L. R.; Belocopitow, E. *Eur. J. Biochem.* **1974**, *42*, 45–50.
(6) Dai, J.; Wang, L.; Allen, K. N.; Radstrom, P.; Dunaway-Mariano, D. *Biochemistry* **2006**, *45*, 7818–24.
(7) Zhang, G.; Dai, J.; Wang, L.; Dunaway-Mariano, D.; Tremblay, L. W.; Allen, K. N. *Biochemistry* **2005**, *44*, 9404–16.
(8) Lahiri, S. D.; Zhang, G.; Dunaway-Mariano, D.; Allen, K. N. *Science* **2003**, *299*, 2067–71.
(9) Blackburn, G. M.; Williams, N. H.; Gamblin, S. J.; Smerdon, S. J. *Science* **2003**, *301*, 1184c.
(10) Allen, K. N.; Dunaway-Mariano, D. *Science* **2003**, *301*, 1184d.
(11) Ahmad, Z.; Senior, A. E. *FEBS Lett.* **2006**, *580*, 517–20.
(12) Antonny, B.; Bigay, J.; Chabre, M. *FEBS Lett.* **1990**, *268*, 277–80.
(13) Antonny, B.; Chabre, M. *J. Biol. Chem.* **1992**, *267*, 6710–8.
(14) Antonny, B.; Sukumar, M.; Bigay, J.; Chabre, M.; Higashijima, T. *J. Biol. Chem.* **1993**, *268*, 2393–402.
(15) Chabre, M. *Trends Biochem. Sci.* **1990**, *15*, 6–10.
(16) Cho, H.; Wang, W.; Kim, R.; Yokota, H.; Damo, S.; Kim, S. H.; Wemmer, D.; Kustu, S.; Yan, D. *Proc. Natl. Acad. Sci. U.S.A.* **2001**, *98*, 8525–30.
(17) Combeau, C.; Carlier, M. F. *J. Biol. Chem.* **1989**, *264*, 19017–21.
(18) Kagawa, R.; Montgomery, M. G.; Braig, K.; Leslie, A. G.; Walker, J. E. *EMBO J.* **2004**, *23*, 2734–44.
(19) Lange, A. J.; Arion, W. J.; Burchell, A.; Burchell, B. *J. Biol. Chem.* **1986**, *261*, 101–7.
(20) Phan, B.; Reisler, E. *Biochemistry* **1992**, *31*, 4787–93.
(21) Schlichting, I.; Reinstein, J. *Nat. Struct. Biol.* **1999**, *6*, 721–3.
(22) Troullier, A.; Girardet, J. L.; Dupont, Y. *J. Biol. Chem.* **1992**, *267*, 22821–9.
(23) Xu, Y. W.; Morera, S.; Janin, J.; Cherfils, J. *Proc. Natl. Acad. Sci. U.S.A.* **1997**, *94*, 3579–83.
(24) The PDB currently contains 33 structures with AlF_3, 49 structures with AlF_4^-, 39 with BeF_3^-, three with BeF_2, and two with BeF_4^{2-}, of which only representative examples are cited.
(25) Wemmer, D. E.; Kern, D. *J. Bacteriol.* **2005**, *187*, 8229–30.
(26) Yan, D.; Cho, H. S.; Hastings, C. A.; Igo, M. M.; Lee, S. Y.; Pelton, J. G.; Stewart, V.; Wemmer, D. E.; Kustu, S. *Proc. Natl. Acad. Sci. U.S.A.* **1999**, *96*, 14789–94.
(27) Martin, R. B. *Biochem. Biophys. Res. Commun.* **1988**, *155*, 1194–200.
(28) Coleman, D. E.; Berghuis, A. M.; Lee, E.; Linder, M. E.; Gilman, A. G.; Sprang, S. R. *Science* **1994**, *265*, 1405–12.
(29) Mittal, R.; Ahmadian, M. R.; Goody, R. S.; Wittinghofer, A. *Science* **1996**, *273*, 115–7.
(30) Rittinger, K.; Walker, P. A.; Eccleston, J. F.; Smerdon, S. J.; Gamblin, S. J. *Nature* **1997**, *389*, 758–62.
(31) Tesmer, J. J.; Berman, D. M.; Gilman, A. G.; Sprang, S. R. *Cell* **1997**, *89*, 251–61.
(32) Madhusudan; Akamine, P.; Xuong, N. H.; Taylor, S. S. *Nat. Struct. Biol.* **2002**, *9*, 273–7.
(33) Baxter, N. J.; Blackburn, G. M.; Marston, J. P.; Hounslow, A. M.; Cliff, M. J.; Bermel, W.; Williams, N. H.; Hollfelder, F.; Wemmer, D. E.; Waltho, J. P. *J. Am. Chem. Soc.* **2008**, *130*, 3952–8.
(34) Graham, D. L.; Eccleston, J. F.; Chung, C. W.; Lowe, P. N. *Biochemistry* **1999**, *38*, 14981–7.
(35) Fletcher, J. I.; Swarbrick, J. D.; Maksel, D.; Gayler, K. R.; Gooley, P. R. *Structure* **2002**, *10*, 205–13.

plexes.[38−40] Given the physiological abundance of magnesium, it is possible that the formation of such complexes may be a relevant feature of the effects of fluoride on enzymes that catalyze phosphate transfer,[41] although generally the mechanisms of fluoride inhibition of magnesium-dependent phosphoryl transfer enzymes are not well defined,[42,43] and Al^{3+} complexes have been shown to form more readily under physiological conditions.[33]

To resolve the controversy concerning the βPGM phosphorane versus TSA assignment, additional data concerning the role and presence of fluoride were required.[44] Further structural studies on βPGM based on ^{19}F NMR analysis showed that the central species was in fact a TSA with a central MgF_3^- moiety (Scheme 1C),[45] consistent with conclusions from theoretical studies[46] and the observation that the activity of βPGM can be inhibited by fluoride.[45] Most recently, ^{19}F NMR has again been used to strongly suggest that structures assigned as AlF_3 are likely to be MgF_3^-, as the magnesium is often present under experimental conditions.[33]

MgF_3^- presents both the correct geometry and the charge to mimic the PO_3^- group in flight, and so is particularly interesting to characterize as a potentially highly accurate TSA. The kinetic analysis of an MgF_3^- adduct is difficult as compared to other metal fluoride TSAs, because it does not, unlike aluminum and beryllium complexes, exist in solution because of its low formation constant and must be assembled and stabilized in the active site.[14,36,45] In this article, we provide a kinetic analysis of fluoride inhibition of βPGM that allows us to measure the stability constant and characteristics of the formation of the TSA. To provide these data, the kinetic scheme previously reported[7] for this enzyme has been refined, which also allowed the species present under the conditions of the structural studies[8,45] to be established and apparent anomalies in inhibition behavior[44] to be deciphered.

Results and Discussion

Fluoride Inhibits Both Activities of βPGM. Figure 1 shows that increasing amounts of fluoride inhibit catalysis by βPGM. First, the ability of βPGM to turn over βG1P to G6P (using a coupled assay for G6P) has already been shown to be inhibited by fluoride.[45] This mutase activity can be conveniently monitored by using a glucose-6-phosphate dehydrogenase (G6PDH)-based coupled assay that converts G6P to 6-phosphogluconolactone,[47] and rates were measured using the linear portions of the change in absorbance of the reaction mixture with time (see below). Given its ready commercial availability, α-glucose-1,6-bisphosphate (αG16BP) has often been used as a convenient cofactor to stimulate βPGM activity despite its stereochemical difference from the bisphosphorylated intermediate (βG16BP) on the reaction pathway.[7,48,49] Adding low concentrations of either αG16BP or βG16BP to the initial reaction mixture accelerates the rate of conversion, but does not affect the fluoride inhibition behavior. However, when high concentrations of the intermediate βG16BP are used, the sensitivity to fluoride is not observed.[44,45]

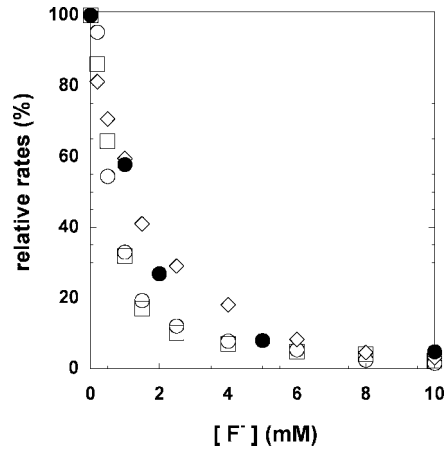

Figure 1. Fluoride inhibits both reactions catalyzed by βPGM. Relative initial rates (%) at 25 °C are shown for the hydrolase activity of βPGM (i.e., converting G6P to glucose, full symbols) and for the mutase reaction of βPGM (i.e., converting βG1P to G6P, open symbols[45]). Reactions contained 2 mM $MgCl_2$, 50 mM buffer (HEPES, pH 7.2), and (●) 5 mM G6P, 10 μM βPGM; (◇) 250 μM βG1P, 200 nM βPGM; (○) 250 μM βG1P, 50 μM αG16BP, 5 nM βPGM; (□) 250 μM βG1P, 0.5 μM βG16BP, 5 nM βPGM.

In addition, a second activity of βPGM is similarly inhibited. βPGM also catalyzes the hydrolysis of G6P to glucose and inorganic phosphate, albeit at much lower rates (Scheme 1B).[7] This hydrolase activity can be monitored using a coupled assay based on glucose dehydrogenase (GDH) and is inhibited with a similar response to fluoride concentration (Figure 1). These initial observations are consistent with formation of a TSA such as MgF_3^-•TSA (Scheme 1C) in the active site of the unphosphorylated form of the enzyme, which competes with binding of the substrates, cofactors, or intermediates and has been structurally characterized.[33,45] If high levels of βG16BP are present, then the free, unphosphorylated enzyme is not present in sufficient concentrations to allow MgF_3^-•TSA to form.[45]

Slow Attainment of Steady State. Although an overall kinetic scheme for βPGM has been established[6,7] (Scheme 1), some features of the kinetic behavior of the system have not yet been described. Most notably, in the simple time course for the reaction of βG1P in the presence of αG16BP cofactor, we observed a lag period of several minutes before a maximal linear response is obtained (Figure 2).[50] This feature is not a consequence of the coupled assay, as the observed rates do not change with increasing concentration of G6PDH. If the reaction mixture is recharged with substrate after the initial substrate has been converted to product, the reaction resumes with a linear

(36) Graham, D. L.; Lowe, P. N.; Grime, G. W.; Marsh, M.; Rittinger, K.; Smerdon, S. J.; Gamblin, S. J.; Eccleston, J. F. *Chem. Biol.* **2002**, *9*, 375–81.
(37) Lee, J. Y.; Yang, W. *Cell* **2006**, *127*, 1349–60.
(38) Toyoshima, C.; Nomura, H.; Tsuda, T. *Nature* **2004**, *432*, 361–8.
(39) Moncoq, K.; Trieber, C. A.; Young, H. S. *J. Biol. Chem.* **2007**, *282*, 9748–57.
(40) Morth, J. P.; Pedersen, B. P.; Toustrup-Jensen, M. S.; Sorensen, T. L.; Petersen, J.; Andersen, J. P.; Vilsen, B.; Nissen, P. *Nature* **2007**, *450*, 1043–9.
(41) Li, L. *Crit. Rev. Oral Biol. Med.* **2003**, *14*, 100–14.
(42) Murphy, A. J.; Coll, R. J. *J. Biol. Chem.* **1992**, *267*, 5229–35.
(43) Murphy, A. J.; Hoover, J. C. *J. Biol. Chem.* **1992**, *267*, 16995–700.
(44) Tremblay, L. W.; Zhang, G.; Dai, J.; Dunaway-Mariano, D.; Allen, K. N. *J. Am. Chem. Soc.* **2005**, *127*, 5298–9.
(45) Baxter, N. J.; Olguin, L. F.; Golicnik, M.; Feng, G.; Hounslow, A. M.; Bermel, W.; Blackburn, G. M.; Hollfelder, F.; Waltho, J. P.; Williams, N. H. *Proc. Natl. Acad. Sci. U.S.A.* **2006**, *103*, 14732–7.
(46) Webster, C. E. *J. Am. Chem. Soc.* **2004**, *126*, 6840–1.
(47) Cosgrove, M. S.; Naylor, C.; Paludan, S.; Adams, M. J.; Levy, H. R. *Biochemistry* **1998**, *37*, 2759–67.
(48) Lahiri, S. D.; Zhang, G.; Dai, J.; Dunaway-Mariano, D.; Allen, K. N. *Biochemistry* **2004**, *43*, 2812–20.
(49) Qian, N.; Stanley, G. A.; Hahn-Hagerdal, B.; Radstrom, P. *J. Bacteriol.* **1994**, *176*, 5304–11.
(50) The observation of kinetics with a lag period has not been mentioned in previous work on βPGM.[7,48]

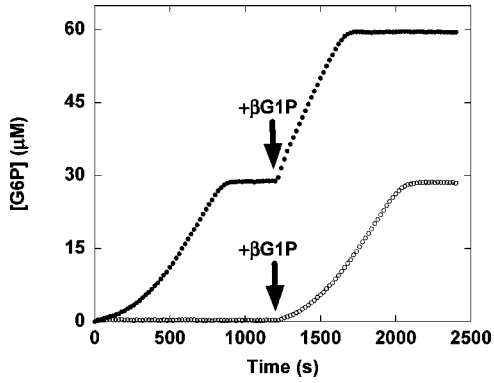

Figure 2. Time courses for the conversion of βG1P to G6P catalyzed by βPGM with αG16BP as a cofactor. The production of G6P was monitored by the increase in absorbance at 340 nm as it reduces NAD^+ in the coupled assay. Two identical solutions containing 5 nM βPGM, 50 μM αG16BP, 5 U/mL G6PDH, 0.5 mM NAD^+, 2 mM Mg^{2+}, and 50 mM buffer (HEPES, pH 7.2) were prepared, and an aliquot of βG1P (final concentration 30 μM) was added to one of them at time zero (●, upper curve). The second solution was incubated under the same conditions (○, lower curve), and no G6P formation was observed. After the reaction was complete, same sized aliquots of βG1P were added to both samples at the time point indicated by the arrows (1200 s). Despite the preincubation with αG16BP, the lower curve shows the same lag as the upper curve in turning over the first aliquot of βG1P. This lag period is not present when the second aliquot is added soon after the first reaction is complete (upper curve).

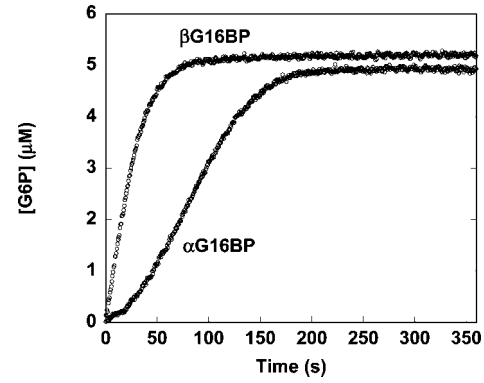

Figure 3. Progress curves for conversion of βG1P to G6P catalyzed by βPGM in the presence of 0.5 μM βG16BP (upper curve) or 100 μM αG16BP (lower curve). The reaction mixtures also contained 10 nM βPGM, 5 μM βG1P, 5 U/mL G6PDH, 0.5 mM NAD^+, 2 mM Mg^{2+}, and 50 mM buffer (HEPES, pH 7.2). The production of G6P was monitored by the increase in absorbance at 340 nm as it reduces NAD^+ in the coupled assay using a stopped-flow spectrophotometer. Only 20% of the data points are shown for clarity.

response and no lag (Figure 2). In keeping with one of the standard assay procedures for these reactions,[7,48,49] 50 μM αG16BP was used as a cofactor in these reactions. One plausible explanation is that this cofactor serves to slowly activate the (initially unphosphorylated[45]) enzyme by converting it to βPGM^P to start the ping-pong mechanism. However, preincubation of βPGM with αG16BP (in the absence of substrate, lower curve in Figure 2) did not eliminate the lag period. As well as confirming that αG16BP is not converted to G6P by βPGM,[7] this experiment suggested that a more likely explanation for the lag is that it represents the accumulation of the βG16BP intermediate (Scheme 1A).

To distinguish these possibilities, we carried out the following experiment: after completely turning over one batch of βG1P, the protein was separated from the small molecule components by filtration through a spin column membrane with a 10 kDa cutoff followed by two washes with buffer. This procedure took less than 10 min, but when the enzyme was immediately incubated with fresh βG1P and αG16BP, the lag period was again apparent. In contrast, if the system is simply recharged with fresh substrate without separation, the lag only appears if an hour or more is allowed to elapse first. Thus, any phosphorylated enzyme that accumulates during the first reaction is rapidly depleted in the absence of a phosporylating agent. If the protein-free fraction is charged with fresh βG1P and fresh enzyme, there is no lag period in the ensuing reaction (upper curve in Figure 2). This suggests that the additional activity of the reaction mixture after reaching steady state is due to the accumulation of a small molecule that is moderately stable under the reaction conditions; the obvious candidate is the βG16BP intermediate.

Qualitatively, the initial nonlinear increase in rate is explained by a mechanism in which the added αG16BP starts off as the most effective reagent for phosphorylating the enzyme. The generation of βPGM^P initiates the ping-pong mechanism: βG1P is converted to βG16BP, which is dephosphorylated either to G6P (and removed by the action of the coupled assay) or back to βG1P. In either case, the total combined concentration of βG16BP and βPGM^P is maintained. This cycle is accelerated as more βPGM^P is generated by the continuing action of αG16BP. The initial phase is effectively converting αG16BP to βG16BP, which is more potent at phosphorylating the enzyme, while simultaneously converting 1 equivalent of βG1P to αG1P until quasi-steady state is achieved. This quasi-steady state depends on the concentrations, binding affinities, and rates of reaction of the two G16BP anomers with βPGM, and the corresponding parameters for the interactions between βPGM^P and the monophosphorylated sugars present. Over a longer time scale, when the βG1P concentration has become much lower, water can compete with the glucose monophosphate species present to dephosphorylate βPGM^P and hence deplete the active components of the system.

When αG16BP is not used as a cofactor, the reaction is much slower, showing that βG1P is a much less effective phosphorylating agent for βPGM.[6] The induction period is still present, but recharging the reaction with fresh substrate soon after turning over a batch of βG1P did not eliminate the nonlinear growth in the subsequent reaction. This suggests that a lower concentration of βG16BP accumulates, as would be expected with a less efficient phosphate donor, and that steady state is not being reached under these reaction conditions.

Synthesis and Use of βG16BP as Cofactor. Although enzymatically generated βG16BP has been used in some studies,[6] most data concerning the kinetic analysis of βPGM have been obtained with commercially available αG16BP.[7,48,49] As described above, this leads to reaction progress curves that are not simple to interpret quantitatively. Hence, we synthesized an authentic sample of βG16BP as outlined in Scheme 2. The β-stereochemistry at the anomeric center is established by the Schmidt coupling[51] using phosphoric acid, and the final stereochemistry by 1D and 2D NMR analysis and comparison with spectra of a commercial sample of αG16BP (see Figure S5 in the Supporting Information).

Initial time courses in the presence of βG16BP (Figure 3) clearly differ from those obtained with αG16BP in two respects. First, no lag period is evident, so a true steady state

(51) Schmidt, R. R.; Stumpp, M.; Michel, J. *Tetrahedron Lett.* **1982**, *23*, 405–408.

Scheme 2. Synthesis of β-D-Glucose-1,6-bisphosphate

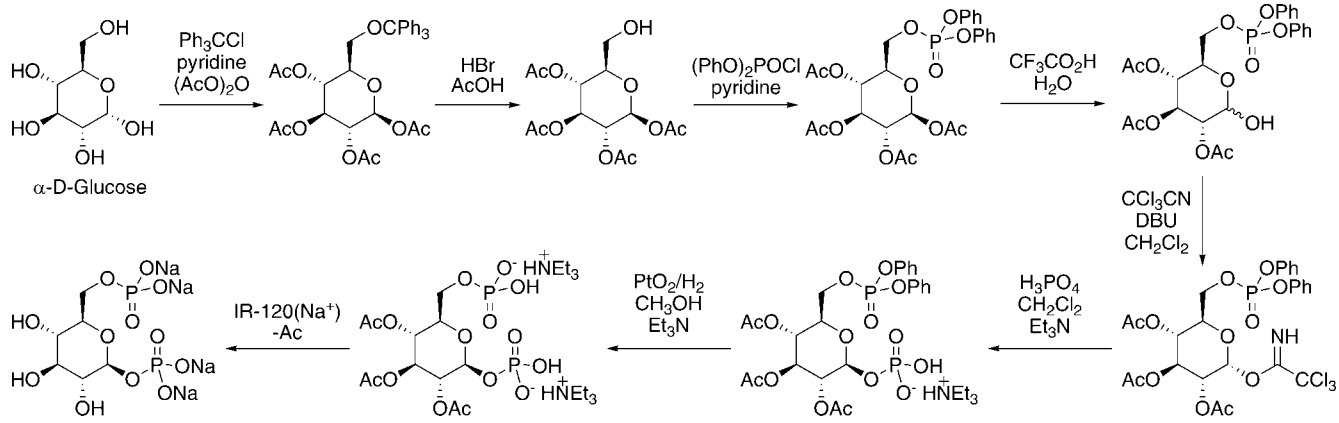

is readily accessible during the initial phase of the reaction. Second, the initial rate is much faster in the presence of βG16BP than αG16BP, indicating that the reaction intermediate βG16BP is a far more effective phosphorylating agent for βPGM, as we had inferred previously. The maximal rate achieved in the presence of 100 μM αG16BP is lower than that for 0.5 μM βG16BP, suggesting that only a very low proportion of the αG16BP is converted into the β anomer. (These data are measured with the cofactors close to or over their respective K_M values; the complex relation between rates and binding of the different species means that we only note these key qualitative observations in this section and describe our quantitative analysis of reaction progress below.) Figure 3 also shows that less G6P is generated when αG16BP is used instead of βG16BP. Under these experimental conditions, once the βG1P has been consumed, any residual βG16BP is converted to G6P only very slowly (as the reaction becomes limited by acyl phosphate hydrolysis of βPGM^P, see below), and so this difference is not due to the added intermediate. As αG16BP is not converted to G6P by βPGM, the only G6P generated in either experiment is derived from the available βG1P. However, αG16BP is converted to αG1P by βPGM, forming βPGM^P that can react with βG1P to form βG16BP. Hence, some αG16BP is converted to βG16BP, which accelerates the conversion, at the expense of reducing the concentration of the substrate βG1P and producing a corresponding concentration of αG1P (which is not detected by the coupled assay). The extent of this conversion is shown by the decrease in the final concentration of G6P produced, as compared to the complete conversion of βG1P that occurs when βG16BP is used as a cofactor. For the experiment shown in Figure 3, this corresponds to about 0.3 μM, which is consistent with the difference in rates of the two experiments.[52]

Presteady-State Kinetics with βG16BP. To obtain direct evidence for the steps postulated in Scheme 1, we undertook a presteady-state analysis using βG16BP as the sole substrate (Figure 4A). A burst was observed prior to the linear steady-state response. The amplitude of the burst was proportional to the concentration of βPGM (Figure 4B), indicating that this reflects a single turnover event involving the enzyme. The observed biphasic behavior is readily accounted for by a mechanism where the enzyme is phosphorylated, generating G6P, which is removed from the system by the coupled assay. Further βG16BP can only be turned over once the βPGM^P produced is hydrolyzed, and so the steady-state linear response represents rate-limiting hydrolysis of βPGM^P. The steady-state velocity is directly proportional to the concentration of βPGM (Figure 4B), but does not depend on the concentration of βG16BP (data not shown), and has a rate constant of 0.026 ± 0.001 s^{-1}. With a half-life of ~30 s, βPGM^P does not persist in aqueous solution in the absence of an efficient phosphate donor, confirming our analysis of the activating species that accumulates in solution during the initial turnover of βG1P (also noted in ref 7).

This instability establishes that αG16BP phosphorylates the enzyme principally by donating phosphate from the 6 position, giving αG1P, which is not detected in the coupled assay.[7] If

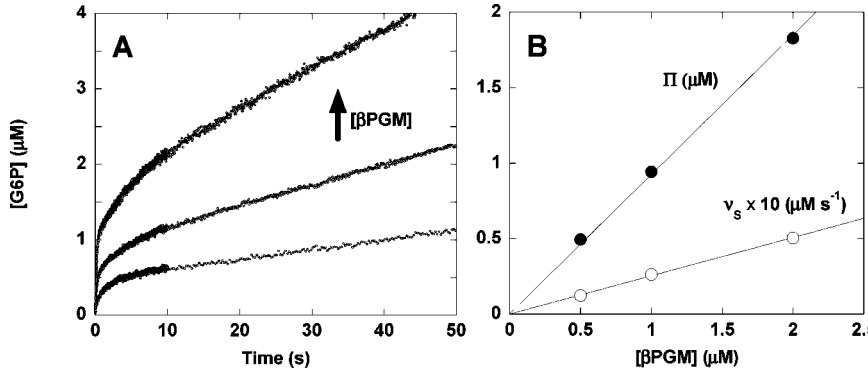

Figure 4. Presteady-state analysis of the conversion of βG16BP to G6P catalyzed by βPGM. (A) The time course of the reaction of 0.5, 1, and 2 μM βPGM with 4.5 μM βG16BP measured by the increase in absorption at 340 nm as the G6P generated reduces NAD^+ in the coupled assay (20 U/mL G6PDH, 2 mM $MgCl_2$, 0.5 mM NAD^+, 50 mM buffer (HEPES, pH 7.2, 25 °C)). (B) The dependence of both the burst amplitude (**Π**) and the steady-state rate (ν_s) obtained from panel A is linear when plotted against βPGM concentration.

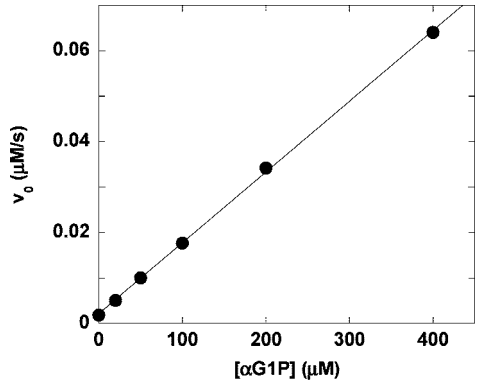

Figure 5. The dependence of the rate of conversion of βG16BP to G6P catalyzed by βPGM on the concentration of αG1P. The production of G6P was monitored by the increase in absorbance at 340 nm as it reduces NAD^+ in the coupled assay. Conditions: 70 nM βPGM, 10 μM βG16BP, 2 mM $MgCl_2$, 5 U/mL G6PDH, 0.5 mM NAD^+, 50 mM buffer (HEPES, pH 7.2) at 25 °C.

Scheme 3. Ping Pong Bi Bi Scheme for the Reaction of βPGM in the Presence of βG16BP as a Cofactor That Incorporates Substrate Inhibition[a]

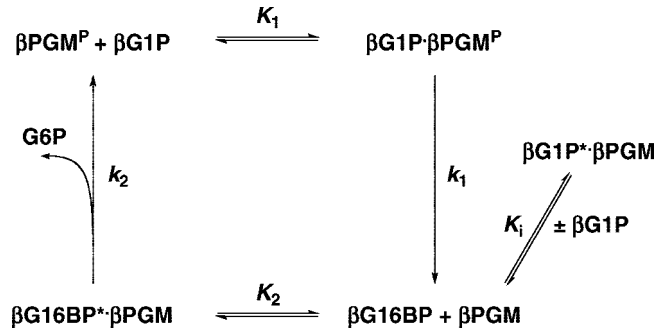

[a] When the βG16BP intermediate binds to βPGM, either the 6-phosphate (βG16BP·βPGM) or the 1-phosphate (βG16BP*·βPGM) is placed at the phosphoryl transfer site. The hydrolase activity is slow in comparison with the isomerase activity when βG16BP is present in the reaction solution as a cofactor, and the removal of G6P by the coupled assay is fast and irreversible.

the 1-phosphate had been donated, then G6P would be formed and generate a signal via the coupled assay; as shown above, the βPGM^P also formed would be readily hydrolyzed back to βPGM, allowing turnover and hence amplification of this reaction. As no G6P is detectable (Figure 2), only a very small proportion of the phosphoryl donation can occur from the 1-position.

The transfer of the phosphoryl group from the 6-position could be monitored in the reverse direction by measuring how added αG1P accelerated the rate of the steady-state reaction when βG16BP was the only substrate (Figure 5). This confirmed that the phosphorylated sugar is a much more effective phosphate acceptor than water. No saturation is observed for this process, and so only a second-order rate constant (2230 ± 30 M^{-1} s^{-1}) can be evaluated for this process. If it is assumed that the hydrolysis reaction is also occurring under subsaturating conditions with respect to water, then the second-order rate constant for hydrolysis would be $(4.7 \pm 0.2) \times 10^{-4}$ M^{-1} s^{-1}, suggesting a differential of about 5×10^6-fold (see below).

Steady-State Kinetics with βG16BP. In the presence of βG16BP, the steady-state initial reaction velocity could be measured easily from the linear response of the assay. Varying both βG16BP and βG1P, substrate inhibition at higher concentrations of βG1P was clearly observable (Figure 6A). This observation has not been previously reported,[7,48,53] and so the proposed Ping Pong Bi Bi mechanism has to be expanded to take this into account (Scheme 3). These steady-state data are globally fit to eq 1, which is derived for a Ping Pong Bi Bi mechanism with substrate inhibition (Scheme 3).[54]

$$v_0 = \frac{k_{cat}[E_T][\beta G1P][\beta G16BP]}{\left([\beta G1P][\beta G16BP] + K_{\beta G1P}[\beta G16BP] + K_{\beta G16BP}[\beta G1P]\left(\frac{K_i + [\beta G1P]}{K_i}\right)\right)} \quad (1)$$

A nonlinear regression program[55] originally written by Duggleby[56] was used for this simultaneous curve fit. The derived parameters are gathered in Table 1 and were used to generate the solid lines in Figure 6. E_T is the total enzyme concentration, $K_{\beta G1P}$ and $K_{\beta G16BP}$ are Michaelis constants for the substrate and cofactor binding to βPGM^P and βPGM, respectively, and K_i is the binding constant for βG1P to βPGM. In this latter complex, βG1P can bind to βPGM with the phosphate group in the distal binding site, presenting the 6-OH into the active site and inhibiting the enzyme. Alternatively, if βG1P is bound with the phosphate group in the active site, it still effectively forms an unproductive complex, as it only transfers the phosphoryl group to the enzyme very slowly relative to the other processes under these conditions. Hence, K_i derived from this scheme will contain contributions from both of these binding modes.

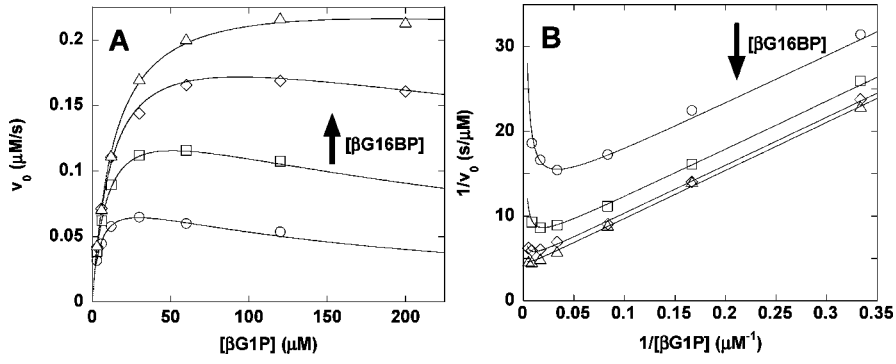

Figure 6. Steady-state analysis of the conversion of βG1P to G6P catalyzed by βPGM in the presence of βG16BP (increasing concentrations shown by arrows). (A) The initial reaction rates vs [βG1P] at different concentrations of βG16BP (0.35, 1.0, 3.5, and 14 μM). Equation 1 was globally fit to the data, and the solid lines show the predicted behavior using the resulting parameters. (B) Lineweaver−Burk plot of the data in panel A. The lines present the solution of the global fit of the appropriate reciprocal version of eq 1 to these data. Conditions: 4 nM βPGM, 5 U/mL G6PDH, 0.5 mM NAD^+, 2 mM $MgCl_2$, 50 mM buffer (HEPES, pH 7.2) at 25 °C.

Table 1. Kinetic Parameters Determined under Steady-State Conditions (from Initial Rates in the Presence of βG16BP) and Non-Steady-State (from Progress Curves in the Presence of αG16BP)

parameter[a]	fit to Scheme 3[b]	fit to Scheme 5[c]	calculated[d]
k_{cat}	$64.7 \pm 0.7\ s^{-1}$		$74 \pm 15\ s^{-1}$
K_m (βG1P)	$14.7 \pm 0.5\ \mu M$		$15 \pm 4\ \mu M$
K_m (βG16BP)	$0.72 \pm 0.04\ \mu M$		$0.8 \pm 0.2\ \mu M$
K_i (βG1P)	$122 \pm 15\ \mu M$	$122 \pm 8\ \mu M$	$122 \pm 8\ \mu M$
k_1		$253 \pm 22\ s^{-1}$	
K_1 (βG1P)		$51 \pm 5\ \mu M$	
k_2		$105 \pm 3\ s^{-1}$	
K_2 (βG16BP)		$1.1 \pm 0.1\ \mu M$	
k_5		$2.9 \pm 0.3\ s^{-1}$	
K_5 (αG16BP)		$91 \pm 6\ \mu M$	
$K_{i\alpha}$ (αG16BP)		$21 \pm 2\ \mu M$	
k_{H2O}[e]	$0.026 \pm 0.001\ s^{-1}$		

[a] The equations used to convert the kinetic parameters from the progress curves to the steady-state parameters are given in the Supporting Information. [b] Steady-state parameters obtained by fitting initial rates to eq 1 based on Scheme 3. [c] Parameters were obtained by fitting progress curves to differential equations based on Scheme 5. [d] Steady-state parameters calculated from the parameters obtained by fitting progress curves to the model described in Scheme 5 as given in the previous column. [e] k_{H2O} determined from steady-state rates when only βG16BP was present in the reaction mixture and the rate-limiting step at steady state is the hydrolysis of phosphoenzyme. Conditions: $[MgCl_2] = 2$ mM, 50 mM buffer (HEPES, pH 7.2).

Scheme 4. Minimal Reaction Scheme for the Reaction of βPGM in the Presence of αG16BP[a]

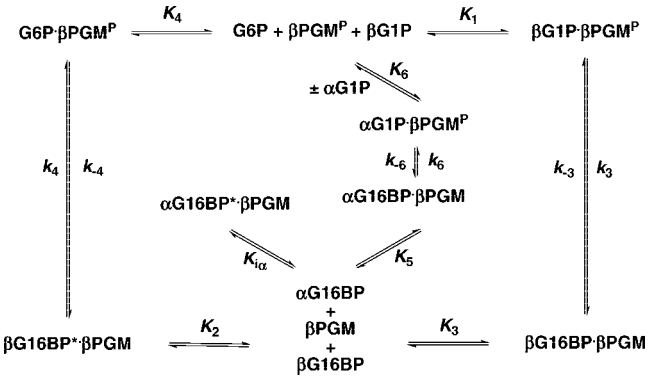

[a] When the βG16BP intermediate binds to βPGM, either the 6-phosphate (βG16BP•βPGM) or the 1-phosphate (βG16BP*•βPGM) is placed at the phosphoryl transfer site. When the αG16BP cofactor binds to βPGM, only the 6-phosphate (αG16BP•βPGM) is productively placed at the phosphoryl transfer site. If the 1-phosphate is placed in the active site, an unproductive complex is formed (αG16BP*•βPGM). The hydrolase activity is slow in comparison with the isomerase activity when α or βG16BP is present in the reaction solution as a cofactor. This scheme is valid for low βG1P substrate concentrations where substrate inhibition can be neglected (see text).

The value for $K_{\beta G1P}$ is in close agreement with earlier reports (14.6 μM).[7,48] For k_{cat}, the same authors reported a range of values between 17.1[7] and 177 s^{-1}.[6] In addition to experimental error (e.g., in determination of the enzyme concentration by Bradford assay),[44] differences to this study are expected due to the handling of the lag period.[7] As a result, different final Michaelis−Menten parameters may arise as the accelerating effect of time-dependent accumulation of βG16BP and the decelerating effect of substrate inhibition will affect the measured conversion rates. More generally, these Michaelis−Menten parameters are not simple binding or rate constants but are composites of several individual constants (see Supporting Information).

Quasi-Steady-State Kinetics with αG16BP. The presence of the lag periods when αG16BP is used as cofactor makes the measurement of initial rates unreliable, so we have analyzed these data using the time courses of the reaction (shown in Figure 7). As with the βG16BP experiments, there is substrate inhibition, as shown by the decrease in the maximal rate at higher substrate concentrations (Figure 7). These data were initially fitted to the kinetic parameters defined in Scheme 4 using the series of differential equations governing each reaction step, with the addition of additional equilibria to account for substrate inhibition as shown in Scheme 3. This direct nonlinear fitting was carried out using DynaFit[57] and carried out simultaneously on the entire set of progress curves for the reaction of different concentrations of βG1P. In this data fitting, we assume that the total concentration of αG16BP and βG16BP

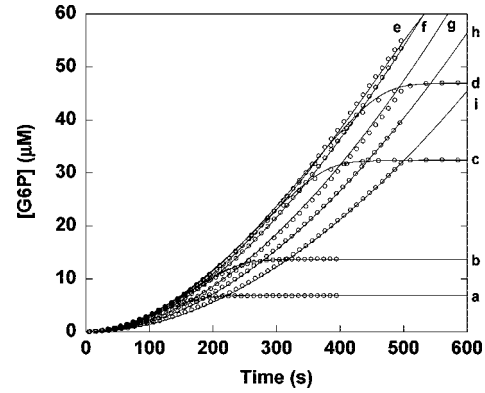

Figure 7. The progress curves for the conversion of βG1P to G6P catalyzed by βPGM in the presence of αG16BP. The black lines represent the solution of globally fitting the differential equations describing the simplified kinetic Scheme 5 to the data. Conditions: 4 nM βPGM, βG1P (7.5 (a), 15 (b), 35 (c), 50 (d), 70 (e), 100 (f), 160 (g), 230 (h), and 330 (i) μM), 50 μM αG16BP, 5 U/mL G6PDH, 0.5 mM NAD^+, 2 mM $MgCl_2$, 50 mM buffer (HEPES, pH 7.2) at 25 °C. Only 1% of the data points are shown for clarity.

Scheme 5. Simplified Reaction Scheme for the Reaction of βPGM in the Presence of αG16BP as a Cofactor That Incorporates Substrate and Cofactor Inhibition[a]

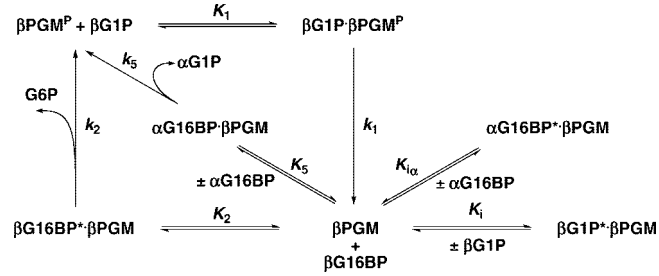

[a] When the βG16BP intermediate binds to βPGM, either the 6-phosphate (βG16BP•βPGM) or the 1-phosphate (βG16BP*•βPGM) is placed at the phosphoryl transfer site. αG16BP can either bind productively (αG16BP•βPGM, with the 6-phosphate at the transfer site) or unproductively (αG16BP*•βPGM, with the 1-phosphate at the transfer site). The hydrolase activity is slow in comparison with the isomerase activity when α or βG16BP is present in the reaction solution as a cofactor, but the removal of G6P by the coupled assay is fast and irreversible.

(52) See the Supporting Information for a discussion about how much βG16BP is formed when αG16BP is used as a cofactor.
(53) Lahiri, S. D.; Zhang, G.; Radstrom, P.; Dunaway-Mariano, D.; Allen, K. N. *Acta Crystallogr., Sect. D: Biol. Crystallogr.* **2002**, *58*, 324–6.
(54) Segel, I. H. *Enzyme Kinetics*; John Wiley & Sons, Inc.: New York, 1993; pp 826−830.
(55) Stojan, J. *Acta Chim. Slov.* **1987**, *34*, 233–241.
(56) Duggleby, R. G. *Comput. Biol. Med.* **1984**, *14*, 447–55.
(57) Kuzmic, P. *Anal. Biochem.* **1996**, *237*, 260–73.

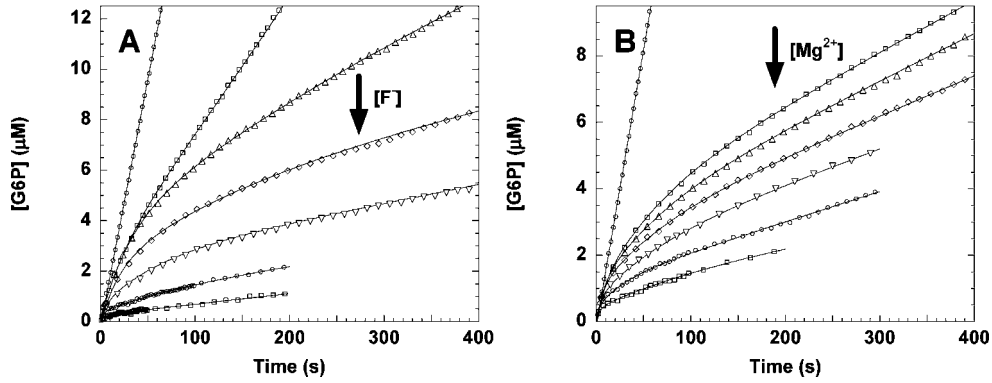

Figure 8. Progress curves for the conversion of βG1P to G6P catalyzed by βPGM in the presence of varying concentrations of Mg^{2+} and F^- (increasing concentrations are denoted by arrows). Conditions: 250 μM βG1P, 0.5 μM βG16BP, 5 U/mL G6PDH, 0.5 mM NAD^+, 50 mM buffer (HEPES, pH 7.2) at 25 °C. (A) 2 mM $MgCl_2$ and 0, 1, 1.5, 2, 3, 5, or 7.5 mM NH_4F; (B) 5 mM NH_4F and 0.3, 0.6, 0.9, 1.2, 1.5, or 2.0 mM $MgCl_2$. Straight curve on the left in both (A) and (B): 2 mM $MgCl_2$ and 0 mM NH_4F. Only 10% of the data points are shown for clarity.

remains constant for the duration of the isomerization from βG1P to G6P, as the phosphoryl transfer process between the glucose species is far faster than the hydrolysis of βPGM^P. However, some intermediates that have to be on the reaction pathway do not accumulate and hence are kinetically invisible. This prevented the fit converging, as the individual constants relating to these intermediates are not defined under these conditions. Therefore, we simplified the reaction scheme by omitting the intermediate complexes $\beta PGM^P \cdot$G6P and βPGM$\cdot\beta$G16BP and replacing the associated individual reactions by a single overall rate constant in each case (Scheme 5). We assume that their lifetimes are very small and negligible as compared to the slower, rate-limiting steps in the overall reaction. For $\beta PGM^P \cdot$G6P, it is reasonable to assume that dissociation is a fast physical process, and because the coupled assay makes this step irreversible, we kinetically omit it, and the transformation of βPGM$\cdot\beta$G16BP to βPGM^P and G6P is represented by the single overall rate constant k_2. For βPGM$\cdot\beta$G16BP, the thermodynamic bias of the system to the G6P products prevents this intermediate from being explicitly included, and so we represent the transformation of $\beta PGM^P \cdot \beta$G1P to βPGM and βG16BP by one overall rate constant k_1. Scheme 5 also includes the equilibrium constant K_i for binding of the substrate to βPGM, to account for substrate inhibition. The model discrimination feature of DynaFit was used to select the best substrate inhibition model. Finally, we found that significantly reduced residuals were obtained when an unproductive binding mode of αG16BP to βPGM was included in the scheme ($K_{i\alpha}$). Our previous experiments have already established that αG16BP does not donate the 1-phosphate group, so it is reasonable to include an unreactive complex where the 6-phosphate is in the distal site and the 1-phosphate is near the active site but is not transferred to the enzyme. Table 1 displays the kinetic parameters calculated by DynaFit through global fitting of all of the progress curves shown in Figure 7 to the model based on these assumptions (shown in Scheme 5).

From these parameters, we have calculated the overall kinetic constants k_{cat} and K_M for comparison with those measured using βG16BP and the conventional steady-state analysis. These are also shown in Table 1 and are in excellent agreement, validating our assumptions in drawing up the kinetic scheme.[58]

Confirming our qualitative conclusions above, we conclude that in the presence of αG16BP the rate-limiting step at the beginning of the reaction is the phosphorylation of the enzyme by αG16BP ($k_5 = 2.9\ s^{-1}$), which is rather slower than the previously reported k_{cat} of 17 s^{-1} using the same cofactor.[7] The larger figure probably results from measurements that include the increase in conversion rate as βG16BP accumulates, typically reaching a quasi-steady state that gives an approximately linear final portion of the progress curve. (See above for comments on the differences in the composite kinetic parameters due to substrate inhibition and nonlinearity of progress curves.) The analysis described here gives a comprehensive quantitative reaction scheme that is compatible with previous observations and provides the framework to investigate the details of fluoride inhibition of βPGM.

Inhibition by Fluoride. The reaction progress curves for the transformation of βG1P to G6P in the presence of increasing amounts of fluoride show increasing deviations from linearity (Figure 8A). Similar behavior is evident if the concentration of magnesium is increased in the presence of fluoride (Figure 8B). This observation can be explained by a time-dependent change of the observed inhibition constant that occurs over a few minutes and suggests the slow binding or formation of an inhibitor that depends on both magnesium and fluoride ions.[59] The curves cannot be fit to a simple burst equation appropriate for a simple slow binding process without leaving significant fitting residuals (see Supporting Information) and so were fit to an equation (eq 2) that mathematically describes slow binding inhibition involving formation of the enzyme−inhibitor complex in two steps (Scheme 6).[60]

$$[P] = v_0^F\left(Y_0 \cdot t + Y_1 \cdot \frac{(1 - e^{-k_a t})}{k_a} + Y_2 \cdot \frac{(1 - e^{-k_b t})}{k_b}\right) \qquad (2)$$

v_0^F is the initial rate of substrate conversion in the presence of fluoride and can be calculated from the modified eq 1 (see Supporting Information), but both exponential factors are the consequence of the slow two-step inhibition mechanism and represent the time-dependent deviation from v_0^F. Values for parameters Y_0, Y_1, Y_2, k_a, and k_b were obtained by nonlinear

(58) Equations for this conversion are given in the Supporting Information. We note that it is very difficult to directly determine these parameters from the individual progress curves obtained in the presence of αG16BP.

(59) The lack of a dependence of the initial rates on magnesium ion concentration on the timescale where the reaction is already fluoride-dependent suggests a sequential model in which fluoride binds first, followed by association of magnesium (Figures S1 and S2).

(60) Sculley, M. J.; Morrison, J. F.; Cleland, W. W. *Biochim. Biophys. Acta* **1996**, *1298*, 78–86.

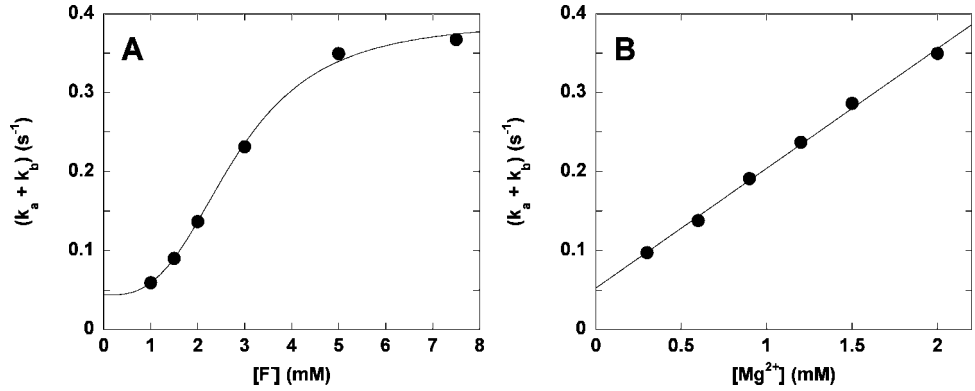

Figure 9. Dependence of $k_a + k_b$ on (A) $[F^-]$ with 2 mM Mg^{2+} present and (B) $[Mg^{2+}]$ with 5 mM F^- present. The solid lines are obtained by fitting the data to eq 4 where (A) $[F^-]$ is variable and $[Mg^{2+}]$ is kept constant and (B) $[F^-]$ is kept constant and $[Mg^{2+}]$ is variable. In both cases, the sum $k_{i2} + k_{i3} + k_{i4}$ is the intercept on the *y*-axis as $[F^-]$ or $[Mg^{2+}]$ goes to zero, respectively.

Scheme 6. Three-Step Mechanism for the Formation of a MgF_3^-•TSA in the Active Site of βPGM

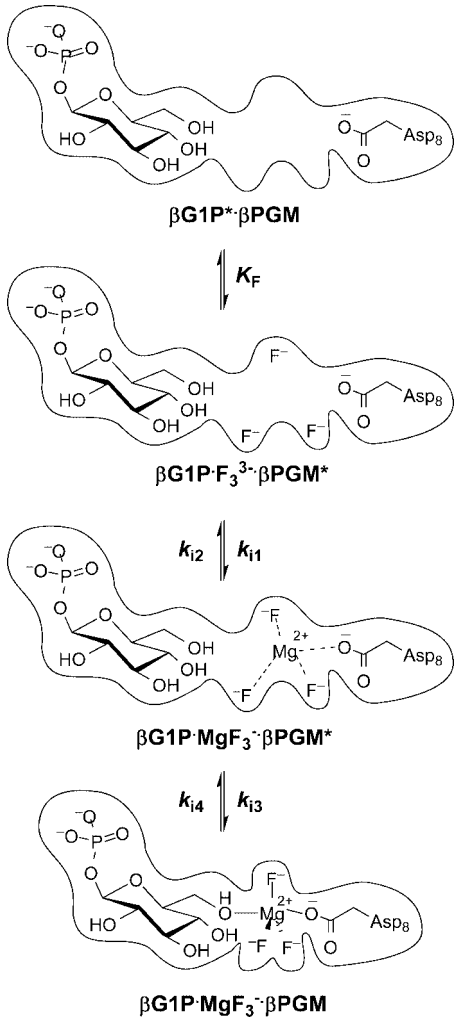

least-squares fitting of each progress curve to eq 2. As these parameters are mathematically related to the rate constants k_{i1}, k_{i2}, k_{i3}, and k_{i4} given in Scheme 6 (see Supporting Information), all four kinetic constants can be calculated (Table 2). The parameters k_a and k_b are also related by eq 3,[60] where I is the slow binding inhibitor.[61]

$$k_a + k_b = k_{i1}[I] + k_{i2} + k_{i3} + k_{i4} \qquad (3)$$

Table 2. Kinetic Constants Calculated from the $(k_a + k_b)$ versus $[F^-]$ and $[Mg^{2+}]$ Plots and the Values of Y_0, Y_1, and Y_2 Determined from the Time-Dependent Inhibition Progress Curves

	fluoride-dependent	magnesium-dependent
K_F (mM)	2.8 ± 0.1	
k_{i1} (M^{-1} s^{-1})	166 ± 10	173 ± 5
k_{i2} (s^{-1})	0.037 ± 0.007	0.035 ± 0.008
k_{i3} (s^{-1})	0.010 ± 0.006	0.011 ± 0.004
k_{i4} (s^{-1})	$(5.6 \pm 1.6) \times 10^{-3}$	$(4.9 \pm 1.6) \times 10^{-3}$

Plotting $k_a + k_b$ against the concentration of fluoride or magnesium ions gives further insight into the process of complex formation (Figure 9A and B). The dependence on magnesium concentration is linear, which means that the inhibitor I in eq 3 is magnesium or a magnesium-containing species. When the fluoride concentration is varied, a nonlinear dependence is observed. This can be fit as a cooperative process (eq 4) and provides a value of $n = 3.3 \pm 0.5$ and an effective binding constant $K_F = 2.8 \pm 0.1$ mM. Constraining the value of n to 3 to reflect a stoichiometric process leads to the fit shown in Figure 9A, with $K_F = 2.8 \pm 0.1$ mM and $k_{i2} + k_{i3} + k_{i4} = 0.051 \pm 0.007$ s^{-1}, again in good agreement with the data in Table 2.

$$k_a + k_b = k_{i1}[Mg]\left(\frac{[F^-]^n}{K_F^n + [F^-]^n}\right) + k_{i2} + k_{i3} + k_{i4} \qquad (4)$$

We can sum up the formation of the inhibitory complex in terms of a sequence of three steps, one fast and two slow, as shown in Scheme 6. A fast cooperative binding of three fluoride ions to the unproductive βG1P*•βPGM complex is followed by a second, slower association of magnesium, before a final slow conformational change generates the more energetically stable closed form. This proposal is consistent with the stoichiometry, cooperative fluoride binding, and conformational change observed in the previous NMR studies for the formation of the TSA shown in Scheme 1C.[45] A similar mechanism has been proposed by Antonny et al. for the activation of transducin and G-proteins by fluoride and magnesium.[12,14]

The K_i for substrate inhibition by βG1P arising from the earlier analysis is 1.22×10^{-4} M, which provides a lower limit

(61) The rate constants k_a and k_b describe the transition from initial to steady state, and their sum is related to the rate-limiting process. At constant βG1P concentration, the initial rates (and the time-dependent deviations from linearity) are functions of fluoride and magnesium concentrations only, as magnesium and fluoride bind with βG1P*•βPGM to form the enzyme−TSA complex.

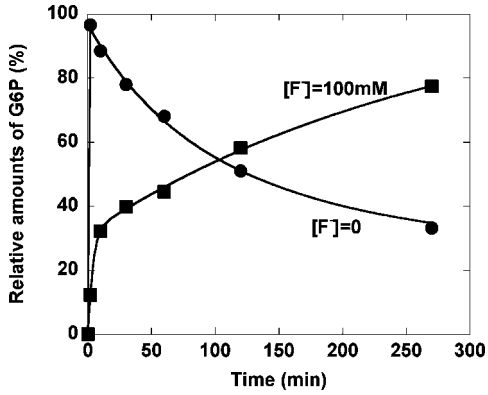

Figure 10. Time course of the conversion of βG1P to G6P catalyzed by βPGM expressed as relative amounts of G6P. 100% represents full turnover of βG1P. In the absence of NH_4F (●), G6P is instantly generated and then slowly hydrolyzed to glucose and inorganic phosphate P_i. In the presence of 100 mM NH_4F (■), the conversion is slowed considerably and generates a biphasic pattern with a fast phase followed by more strongly inhibited turnover. Conditions: 0.22 mM βPGM, 6 mM βG1P, 10 mM $MgCl_2$, 1 mM DTT, 50 mM buffer (HEPES, pH 7.2).

on the dissociation constant of the substrate from βPGM when it is bound in an orientation suitable for forming the TSA as shown in Scheme 6.[62] This defines the concentration of enzyme that can bind to the inhibitor, which is applicable to the above analysis. The fits described above give an overall K_D for the binding of three fluoride ions to this species of 2.2×10^{-8} M^3, and a dissociation constant for magnesium from the TSA of $(k_{i2} \times k_{i4})/(k_{i1} \times (k_{i3} + k_{i4})) = 60$ μM. The product of all three constants gives the overall dissociation constant of βG1P·MgF_3^-·βPGM into its individual components in solution as $K_{TSA} \leq 2 \times 10^{-16}$ M^5.

Evidence for Formation of a TSA under Crystallization Conditions. We complemented these kinetic studies by examining the binding behavior of βPGM under conditions similar to those used for crystallization in the presence of fluoride.[8,53] These conditions differ from the kinetic studies in that the G6P product can accumulate as it is not removed by the coupled assay.

The first experiment was carried out by discontinuously measuring the conversion of βG1P to G6P over time in the absence and presence of fluoride (Figure 10). In the absence of fluoride, we observe that βG1P is converted into G6P during the dead time of the experiment (i.e., approximately 10 s, Figure 10) followed by slower hydrolysis over a few hours to leave glucose and inorganic phosphate P_i.[7,45] This fast isomerization is consistent with the previous observation of instant conversion of βG1P to G6P by ^{31}P NMR.[45] In the presence of fluoride, the conversion is markedly slower and clearly biphasic. The biphasic pattern can be explained by the formation of a more tightly bound TSA incorporating MgF_3^- with G6P in place of βG1P in the active site of βPGM. In this scenario, the more efficient longer-term fluoride inhibition is the consequence of the first fast phase when βG1P is partly transformed to G6P. Of further significance is that the system containing fluoride maintains the presence of phosphosugars, as the fluoride inhibits the hydrolase activity of βPGM; this observation is consistent with formation of the TSA complex. On the time scale of crystal growth (i.e., a few days[53]), there would be no phosphosugar in solution if fluoride was absent, and for this reason fluoride is essential for cocrystallization of G6P or βG1P with βPGM.[10]

Table 3. Concentrations of βPGM and G6P in the Supernatant and Flow-Through Solutions in the Presence and Absence of Fluoride

	$[NH_4F] = 0$ mM	$[NH_4F] = 100$ mM
[βPGM] supernatant (retained by membrane)	0.556 ± 0.010 mM	0.634 ± 0.004 mM
[G6P] supernatant (retained by membrane)	0.166 ± 0.008 mM	0.605 ± 0.010 mM
[G6P] flow-through (passed through membrane)	0.176 ± 0.06 mM	0.058 ± 0.006 mM

The initial concentrations of the reagents were 0 or 100 mM NH_4F, 0.46 mM βPGM, 1 mM G6P, 10 mM $MgCl_2$, 1 mM DTT, 50 mM buffer (HEPES, pH 7.2).

In a second experiment, we tried to find out if G6P binds more tightly to βPGM in the presence of fluoride. We used a simple filtration assay with separation by molecular weight in a spin column to separate the G6P in solution from that bound to βPGM under conditions identical to those under which crystals were grown.[8,53,63] Thus, G6P was incubated with βPGM in the presence of 0 and 100 mM fluoride. After filtration through a membrane impermeable to species with molecular weights above 10 kDa, we separated the supernatant and filtered fractions and performed an assay for G6P on each. The ratio of the G6P concentrations reports on how much of the G6P is retained by the enzyme. In the absence of fluoride, equal concentrations of G6P end up in flow-through and supernatant (Table 3), confirming that G6P is only weakly bound by βPGM. This situation is reversed in the presence of fluoride, when a 10-fold higher concentration of G6P is detected in the supernatant. This means that fluoride induces much stronger retention of G6P by βPGM, consistent with the existence of a TSA complex that contains G6P.[64]

It appears that cocrystallization of G6P with βPGM requires the presence of fluoride, leading to a situation where the enzyme is inhibited and the phosphosugar is preserved through being stably but unproductively bound to the enzyme (i.e., as part of the TSA). These findings may explain why it has not been possible to grow crystals containing βG1P or G6P in the absence of fluoride.[10,53]

Conclusions

Ground-State Binding. Of all of the small, stable molecules tested, βPGM shows the highest affinity for the intermediate βG16BP ($K_D = K_2 = 1.1$ μM, consistent with a previous report concerning a βPGM).[65] The weakest affinity measured is for binding the βG1P substrate to the unphosphorylated enzyme ($K_D = K_i = 122$ μM), showing that the second phosphoryl group enhances ground-state binding by about 2.7 kcal mol^{-1}. αG16BP binds with similar affinities in two modes: in an unproductive position ($K_D = K_{i\alpha} = 21$ μM) and in an orientation that allows it to phosphorylate the enzyme with the phosphate in the 6-position ($K_D = K_5 = 91$ μM). These data can be combined to

(62) As noted earlier, this parameter will also include a contribution from βG1P binding with the phosphate in the active site.

(63) Lahiri, S. D.; Zhang, G.; Dunaway-Mariano, D.; Allen, K. N. *Biochemistry* **2002**, *41*, 8351–9.

(64) There is no specific retention of the small molecule species by the membrane. In the absence of βPGM, we find that G6P product can freely diffuse through the membrane, leading to equal concentrations in supernatant and flow-through. When βPGM is filtered, no protein is detected in the flow-through, and the concentration in the supernatant is independent of fluoride.

(65) Marechal, L. R.; Oliver, G.; Veiga, L. A.; de Ruiz Holgado, A. A. *Arch. Biochem. Biophys.* **1984**, *228*, 592–9.

give an observed binding constant of 17 μM to compare with the parameter for βG16BP given above (which also includes dual binding modes), illustrating that the change of the phosphate stereochemistry reduces the weighted average of the binding strength by about 1.6 kcal mol^{-1}. The binding of βG1P ($K_D = K_I = 51$ μM) with βPGM^P appears to be significantly greater than that for αG1P, as no observable deviation from linearity is observed for the reaction of βPGM^P with up to 400 μM αG1P (Figure 5), implying that K_D is at least 4 mM (i.e., ~100 fold weaker) and suggesting that the stereochemical difference perturbs the binding strength by at least 2.7 kcal mol^{-1} in this context.

Transition-State Binding. The interactions between the cap domain and glucose phosphate have been suggested to be important for the function of βPGM, and the greater affinities for bis-phosphorylated sugars indicate that this phosphate is an important binding anchor. In terms of the contribution to catalysis, we can compare the effect of phosphorylation at the 6-position of glucose on the rate of transfer of phosphate from the 1-hydroxyl to βPGM. Using the parameters given in Table 1, k_2/K_2 for the phosphorylation of βPGM by βG16BP = 10^8 M^{-1} s^{-1}. From the k_{cat}/K_M for activation of βPGM by βG1P, the corresponding rate for the monophosphorylated glucose is 710 M^{-1} s^{-1}.[66] Thus, the distal binding site leads to 7.1 kcal mol^{-1} stabilization of the transition state (~140 000-fold rate acceleration), an enhancement of 4.4 kcal mol^{-1} (~1000 fold) as compared to the ground-state interactions of the same species. The same data for phosphorylation of the enzyme by αG16BP give $k_5/K_5 = 3 \times 10^4$ M^{-1} s^{-1}. This comparison suggests a rate difference of ~3000-fold for this phosphate donor, but involves transfer from the 6-position only, and so a different hydroxyl group is involved as compared to βG1P. We can make a related set of comparisons of k_{cat}/K_M for the transfer of phosphate from βPGM^P to various acceptors: 5×10^6 M^{-1} s^{-1} (βG1P; k_1/K_1, Table 1); 2×10^3 M^{-1} s^{-1} (αG1P); and 5×10^{-4} (H_2O). These respective transition states are stabilized by 13.6 kcal mol^{-1} (βG1P) and 9.0 kcal mol^{-1} (αG1P) relative to water. The rate difference between the hydrolysis rate and the transfer to βG1P is about 10^{10}, which is essentially the same rate factor as observed for analogous transformations involving αPGM.[67] The sensitivity to the structures and their stereochemistry is much more pronounced in the transition states than for the binding of the ground-state molecules and may plausibly reflect a role in positioning the Asp10 residue to facilitate the reaction as has been previously suggested,[7] or more effective recognition interactions being expressed as the geometry of the transition state is reached. The magnitude of the contribution from the binding of the distal phosphate is similar to recent analyses from Richard et al. in examining the reactions of TIM and orotate decarboxylase where the phosphate binding locates a loop that enfolds the substrate providing up to 12 kcal mol^{-1} of transition-state stabilization.[68−71] In this case, the same type of interaction facilitates the movement of two larger domains together, rather than the binding of smaller loops.

Fluoride Inhibition and Structural Studies. Previously, it has been reported that fluoride does not inhibit catalysis by βPGM.[10,44] We explained this observation qualitatively by pointing out that if βPGM is kept phosphorylated at Asp8 (by high concentrations of βG16BP), then the TSA cannot form.[45] We can now underline the observations quantitatively.

Zhang et al.[7] have measured kinetics with substrate concentrations up to 75 μM ($0.5K_M$−$5K_M$) at relatively high concentrations of bisphosphate activator ([αG16BP] = 30−100 μM). At these relatively low concentrations of βG1P (i.e., <120 μM where substrate inhibition is not observed), the substrate is not bound to a significant extent to the dephosphoenzyme because of its high K_i, and so the MgF_3^-•TSA complex does not form. Because of the coupled reaction used for monitoring the reaction, the complex with G6P cannot be formed, because G6P is removed continuously by G6PDH and therefore does not accumulate. Second, the fluoride inhibition is a slow process (occurring on a time scale of minutes, see above) and can be missed, if the depletion of the substrate is faster than the complex formation. This can happen at low substrate concentrations and high concentrations of βG16BP.[44]

We note that most of the analysis here concerns the formation of a TSA analogue that uses βG1P, whereas the structurally analyzed complexes contained G6P. This is because our kinetic method uses a coupled assay that removes G6P from the reaction mixture. The preference for the TSA-containing G6P may reflect a higher affinity for this sugar component when it is present, or may simply reflect the greater concentration of this component when equilibrium between βG1P and G6P has been reached.

The slow binding nature of the inhibition process is explained in terms of a conformational change that leads to the final assembly of the TSA complex. This is consistent with the requirement for the two domains of βPGM to fold together to encapsulate the substrate that has been observed crystallographically and by NMR.[7,45] From the parameters that we have measured (k_{i3} and k_{i4} in Table 2), this final conformational change is predicted to have a ratio of about 2:1 for the two forms (βG1P•MgF_3^-•βPGM* and βG1P•MgF_3^-•βPGM in Scheme 6). However, it is possible that conformational changes other than cap domain movement lead to the observed time-dependent inhibition pattern.

We note that several transition-state analogues have been reported to exhibit slow-binding kinetic inhibition characteristics. This isomerization process has been similarly ascribed to a conformational change of the protein and has been related to a mismatch of TSA and enzyme in the initial encounter complex that leads to a suboptimal dynamic response.[72−74]

In terms of resolving the assignment of the original structure, it is now also clear that there is very limited persistence of any phosphorylated glucose unless fluoride is present, especially at the high concentrations of enzyme required for structural studies. Thus, as well as the solution NMR characterization of the TSA

(66) This effective second-order rate constant for phosphorylation of the protein by βG1P was calculated from a plot of initial rates v_o (obtained in the absence of any sugar bisphosphate cofactor) against [βG1P] (see Supporting Information, Figure S6). A similar value of the second-order rate constant can be obtained using data from ref 6. From the turnover number for activation of βPGM by βG1P (0.8 s^{-1}) and the binding constant between βG1P and βPGM (1.2×10^{-4} M, Table 1), the corresponding rate for the monophosphorylated glucose can be calculated as 2×10^3 M^{-1} s^{-1}.

(67) Ray, W. J., Jr.; Long, J. W.; Owens, J. D. *Biochemistry* **1976**, *15*, 4006–17.

(68) Morrow, J. R.; Amyes, T. L.; Richard, J. P. *Acc. Chem. Res.* **2008**, *41*, 539–48.

(69) Amyes, T. L.; Richard, J. P. *Biochemistry* **2007**, *46*, 5841–54.

(70) Amyes, T. L.; Richard, J. P.; Tait, J. J. *J. Am. Chem. Soc.* **2005**, *127*, 15708–9.

(71) Barnett, S. A.; Amyes, T. L.; Wood, B. M.; Gerlt, J. A.; Richard, J. P. *Biochemistry* **2008**, *47*, 7785–7.

(72) Kurz, L. C.; Weitkamp, E.; Frieden, C. *Biochemistry* **1987**, *26*, 3027–32.

(73) Mader, M. M.; Bartlett, P. A. *Chem. Rev.* **1997**, *97*, 1281–1302.

(74) Morrison, J. F.; Walsh, C. T. *Adv. Enzymol. Relat. Areas Mol. Biol.* **1988**, *61*, 201–301.

that is formed, the components required for the formation of a phosphorane species do not persist under the experimental conditions. As has been explained by Tremblay et al.,[44] the species that is bound to the enzyme has to occupy the active site prior to crystallization, as the structure is maintained in the domain−domain closed conformation when the enzyme is crystalline. In the presence of fluoride, the TSA can and does form in solution[45] and so can crystallize. However, in the absence of this inhibitory complex, the proposed phosphorane does not form as the substrate is converted to glucose and inorganic phosphate.

TSA Affinity. The overall dissociation constant of the TSA from the enzyme and into its component parts apparently reflects a very high affinity ($\sim 2 \times 10^{-16}$ M^5) for the enzyme, with the units of M^5 reflecting the multiple components it is made up of (i.e., this constant describes the equilibrium between TSA and βPGM, βG1P, Mg^{2+}, and three F^- ions). By way of comparison, Najjar studied the fluoride inhibition of rabbit muscle α-phosphoglucomutase and found it to be dependent on the concentrations of three different ions, magnesium, fluoride, and glucose-1-phosphate.[75] Inhibition constants were determined by varying the concentration of each ion successively (while leaving the other two unchanged) and combined to give an apparent overall binding constant of 2×10^{-12} M^4 (calculated from $K_i = [Mg^{2+}][F^-]^2[G1P] \times$ (residual activity)/(inhibited activity)).[75] Comparing the numerical values for the inhibition constants, this value is 4 orders of magnitude higher than the K_D for βPGM, although the different dimensions mean that a simple comparison cannot be made. The limited data and different analysis in the earlier work preclude more detailed comparison of these data, although it is plausible that a similar complex also forms in the αPGM with a comparable formation constant.

We can estimate the affinity of the MgF_3^- component for the βPGM complex by taking into account the K_i (1.22×10^{-4} M) for the unproductive βG1P*·βPGM complex, which provides a value of 1.4×10^{-12} M^4 for the dissociation of the MgF_3^- from the TSA and into its individual components. To evaluate the direct affinity between this fragment and the βG1P*·βPGM, we have to estimate the formation constant for MgF_3^-, as it has not been observed in solution. MgF^+ has an association constant of 50 M^{-1}, and for MgF_2, the overall association constant is less than 1.6×10^3 M^{-2} (see ref 76); making a conservative estimate that the binding constant for the third fluoride is the same as for the second (i.e., <30 M^{-1}) leads to a value for the association constant to form MgF_3^- of less than 5×10^4 M^{-3}. This generates an estimate for the dissociation constant of MgF_3^- from the TSA of <70 nM ($(5 \times 10^4) \times (1.4 \times 10^{-12})$), in a range similar to other TSAs.[73]

The instability of MgF_3^- in solution means that its directly observed inhibitory properties are less potent than, for example, the corresponding aluminum fluoride complexes, which have a much higher formation constant in solution and are tighter binding inhibitors of βPGM.[33] However, to provide a reliable basis for the extrapolation from TSA structures to TS structures, the TSA must accurately reflect the geometry and charge distribution of the true TS; the inhibition constant is not a sufficiently good measure to evaluate this fit, which should be based on correlations between the inhibition constant and catalytic parameters.[73,77] For example, in studying the biological catalysis of phosphate transfer, vanadate esters have been used extensively as TSAs,[78] as they readily form trigonal-bipyramidal structures that reflect the geometry of the TS. However, the lack of a correlation between inhibition constants and catalytic parameters for wild type and mutated enzymes suggests that these are not true TSAs.[79,80] This disconnect can be rationalized if the binding characteristics of vanadate do not precisely match transition-state recognition, even though the geometry of the analogue may be accurate. For example, binding of the nonbridging oxygen atom and the strengths of the covalent bonds made directly to the vanadate center may be balanced differently, as the character of these bonds will be different from the partial covalent bonds of the transition state. Thus, the most stable structure of the vanadate−enzyme complex (which optimizes this balance) need not reflect the structure of the TS−enzyme complex. In the context of metal fluoride complexes, the nature of the coordinate bonds between the metal ion and the glucose hydroxyl and asparte oxygens will directly affect the affinity and properties of the complex in a similar fashion, as will the interactions of the coordinated fluorides with the local protein structure. How well these mimic the partial bonding and recognition interactions of the transition state will require further study.

Materials and Methods

Synthesis. All chemicals were obtained commercially (Fluka, Sigma), except for βG16BP, which was synthesized according to Scheme 2 in eight steps.

1,2,3,4-Tetra-*O*-acetyl-6-*O*-triphenylmethyl-β-D-glucose.[81] Anhydrous α-D-glucose (12.0 g, 67 mmol) and triphenylmethyl chloride (19.3 g 69 mmol) were dissolved in anhydrous pyridine (50 mL) by warming on a steam bath (80−100 °C). Acetic anhydride (30 mL) was poured in one portion into the pyridine solution without cooling. The solution was allowed to cool to room temperature and kept at that temperature for an additional 12 h. The above mixture was then introduced in a thin stream into a mixture of ice water (950 mL) and acetic acid (50 mL) while rapidly swirling the container. After 2 h of vigorous agitation, the precipitate was isolated by filtration. To remove residual pyridine, the gummy filter cake was immediately introduced into fresh ice water (1 L), and the mixture was stirred for an additional 20 min. White precipitate was isolated by filtration and subsequently washed with copious amounts of fresh water. As a means to preferentially remove the β-isomer, which has higher solubility in diethyl ether, the crude, air-dried product was then introduced into diethyl ether (50 mL). The less soluble α-isomer was isolated and recrystallized from hot 95% ethanol. Upon cooling, fine needle forms of crystalline 1,2,3,4-tetra-*O*-acetyl-6-*O*-triphenylmethyl-β-D-glucose were liberated; yield 16.2 g (41%). ^{1}H NMR (250 MHz, $CDCl_3$) δ/ppm 7.43 (m, 6H, Ar−H), 7.21−7.40 (m, 9H, Ar−H), 5.73 (m, 1H, C1−H), 5.07−5.30 (m, 3H), 3.69 (m, 1H), 3.33 (dd, $J = 2.4$ and 10.5 Hz, 1H, C*H*H), 3.05 (dd, $J = 4.3$ and 10.7 Hz, 1H, CH*H*), 2.15 (s, 3H, CH_3), 2.04 (s, 3H, CH_3), 2.00 (s, 3H, CH_3), 1.73 (s, 3H, CH_3). ^{13}C NMR (63 MHz, $CDCl_3$) δ/ppm 170.28 (C═O), 169.38 (C═O), 169.01 (C═O), 168.95 (C═O), 143.47 (3C, quarter C in Ph), 128.72 (6C in Ph), 127.80 (6C in Ph), 127.04 (3C in Ph), 91.92 (C1), 86.63 (O−*C*Ph3), 74.05, 73.18, 70.52, 68.28, 61.61 (*C*H_2O), 20.90 (CH_3), 20.67 (CH_3), 20.64 (CH_3), 20.47 (CH_3). TOF MS (ES^+) 613 (M^+ + Na), 243 (100%, Ph_3C^+).

(75) Najjar, V. A. *J. Biol. Chem.* **1948**, *175*, 281–290.
(76) Fovet, Y.; Gal, J. Y. *Talanta* **2000**, *53*, 617–626.
(77) Wicki, J.; Williams, S. J.; Withers, S. G. *J. Am. Chem. Soc.* **2007**, *129*, 4530–1.
(78) Davies, D. R.; Hol, W. G. *FEBS Lett.* **2004**, *577*, 315–21.
(79) Deng, H.; Callender, R.; Huang, Z.; Zhang, Z. Y. *Biochemistry* **2002**, *41*, 5865–72.
(80) Messmore, J. M.; Raines, R. T. *J. Am. Chem. Soc.* **2000**, *122*, 9911–9916.
(81) Lee, G. S.; Lee, Y. J.; Choi, S. Y.; Park, Y. S.; Yoon, K. B. *J. Am. Chem. Soc.* **2000**, *122*, 12151–12157.

1,2,3,4-Tetra-*O*-acetyl-β-D-glucose.[81] 1,2,3,4-Tetra-*O*-acetyl-6-*O*-triphenylmethyl-β-D-glucose (7.4 g, 12.5 mmol) was dissolved in glacial acetic acid (35 mL) by warming on a water bath (heated to 70 °C). The solution was cooled to 10 °C, and then the glacial acetic acid solution of hydrogen bromide (33%, 2.7 mL) was added and the mixture was shaken for 45 s. The liberated triphenylmethyl bromide was immediately removed by suction filtration, and the filtrate was poured in one portion into ice water (150 mL). The glucose tetraacetate was extracted with chloroform (4 × 40 mL), washed with cold water (15 mL × 4), and dried over anhydrous magnesium sulfate. The solvent was removed in vacuo, and then anhydrous diethyl ether (15 mL) was added to the syrupy residue. Crystallization began immediately upon rubbing the syrup using a glass rod. After filtration, 3.4 g (yield 78%) of white solid was obtained. ^{1}H NMR (250 MHz, $CDCl_3$) δ/ppm 5.70 (d, J = 8.24 Hz, 1H, C1−H), 5.28 (t, J = 9.5 Hz,1H), 5.07 (m, 2H), 3.75 (m, 1H), 3.53−3.66 (m, 2H), 2.31 (m, 1H), 2.09 (s, 3H, CH_3), 2.05 (s, 3H, CH_3), 2.01 (s, 3H, CH_3), 2.00 (s, 3H, CH_3). ^{13}C NMR (63 MHz, $CDCl_3$) δ/ppm 170.24 (C═O), 170.09 (C═O), 169.26 (C═O), 169.07 (C═O), 91.71 (C1), 74.90, 72.61, 70.38, 68.16, 60.81 (CH_2O), 20.79 ($2CH_3$), 20.57 ($2CH_3$). TOF MS (ES^+) 371 (100%, M + Na^+), calculated for $C_{14}H_{20}O_{10}$ MW 348.

1,2,3,4-Tetra-*O*-acetyl-β-D-glucose-6-diphenylphosphate.[82] Diphenyl phosphochloridate (0.822 g, 3 mmol) was dissolved in dry pyridine (0.5 mL), and this solution was added slowly to 1,2,3,4-tetra-*O*-acetyl-β-D-glucose (1.04 g, 3 mmol) in dry pyridine (3 mL) at 0 °C. The reaction begins within a few minutes, and a copious crystalline precipitate forms. After addition was complete, the reaction was continued for 1 h at 0 °C and 4 h at room temperature. The solution was poured into 20 mL of cold water, and the pH of the solution was adjusted to about 6 by slowly adding HCl (1 M), and then extracted with CH_2Cl_2 (4 × 30 mL). The extract was washed with cold water (15 mL × 2) and dried over Na_2SO_4. After being concentrated, the crude product was purified by a short column, to yield a colorless oil, 1.665 g, 96% yield. ^{1}H NMR (250 MHz, $CDCl_3$) δ/ppm 7.24 (m, 4H, Ar−H), 7.12−7.15 (m, 6H, Ar−H), 5.65 (d, J = 8.2 Hz, 1H, C1−H), 5.17 (t, J = 9.16 Hz, 1H), 5.01 (m, 2H), 4.14−4.34 (m, 2H), 3.77−3.80 (m, 1H), 2.00 (s, 3H, CH_3), 1.95 (s, 3H, CH_3), 1.93 (s, 3H, CH_3), 1.92 (s, 3H, CH_3). ^{13}C NMR (63 MHz, $CDCl_3$) δ/ppm 170.00 (C═O), 169.21 (C═O), 169.09 (C═O), 168.69 (C═O), 150.30 (d, J = 6.68, 2C), 129.77 (4C), 125.45 (2C), 120.10 (d, 4C), 91.45 (C1), 72.97 (d, J =7.63 Hz, 1C), 72.63, 70.04, 67.82, 66.34 (d, J = 5.72 Hz, CH_2), 20.64 ($2CH_3$), 20.47 ($2CH_3$). ^{31}P NMR (101 MHz, $CDCl_3$) δ/ppm −11.60. TOF MS (ES^+) 603 (100%, M + Na^+), calculated for $C_{26}H_{29}O_{13}P$ MW 580.

2,3,4-Tri-*O*-acetyl-D-glucose-6-diphenylphosphate.[83] A mixture of 1,2,3,4-tetra-*O*-acetyl-α-D-glucose-6-diphenylphosphate (1 g, 1.72 mmol) and trifluroacetic acid (5 mL) was stirred at room temperature for 24 h. Water (0.7 mL) was then added, and the mixture was concentrated in vacuo, keeping the temperature below 35 °C. Toluene (10 mL × 4) was added, and the solution was evaporated in vacuo to remove traces of water, forming a slightly yellowish oil, 685 mg, 74%. ^{1}H NMR (250 MHz, $CDCl_3$) δ/ppm 7.20−7.30 (m, 4H, Ar−H), 7.09−7.14 (m, 6H, Ar−H), 5.43 (dd, J = 9.5 and 9.8 Hz, 1H), 5.19 (d, J = 3.7 Hz, 1H, C1−H), 4.89−4.98 (m, 2H), 4.65 (dd, J = 3.7 and 10.2 Hz, 1H, C2−H), 4.09−4.28 (m, 4H), 1.97 (s, 3H, CH_3), 1.93 (s, 3H, CH_3), 1.91 (s, 3H, CH_3). ^{13}C NMR (63 MHz, $CDCl_3$) δ/ppm 170.23 (2C═O), 169.57 (C═O), 150.34 (m, 2C), 129.84 (4C), 125.56 (2C), 120.09 (d, 4C), 89.81 (C1), 72.67 (d, J = 17.17 Hz, 1C), 71.02, 70.01, 67.27 (d, CH_2), 20.70 ($2CH_3$), 20.59 (CH_3). ^{31}P NMR (101 MHz, $CDCl_3$) δ/ppm −11.83. TOF MS (ES^+) 561 (M + Na^+), calculated for $C_{24}H_{27}O_{12}P$ MW 538. This product was used for the next step without further purification.

2,3,4-Tri-*O*-acetyl-α-D-glucose-6-diphenylphosphate-1-trichloroacetimidate.[84] 2,3,4-Tri-*O*-acetyl-D-glucose-6-diphenylphosphate (685 mg) was dissolved in dry dichloromethane (10 mL), and trichloroacetonitrile (2 mL) was added at room temperature. The reaction started after a few drops of 1,8-diazobicyclo[5.4.0]undec-7-ene (DBU) were added to this mixture. After 1 h of stirring, the resulting brown mixture was concentrated in vacuo and was purified by a short column (petroleum ether:ethyl acetate 3:1 to 1:1), to yield a yellowish oil, 713 mg, 82%. ^{1}H NMR (250 MHz, $CDCl_3$) δ/ppm 8.65 (s, 1H, NH), 7.33 (m, 4H, Ar−H), 7.14−7.19 (m, 6H, Ar−H), 6.49 (d, J = 3.7 Hz, 1H, C1−H), 5.52 (t, J = 9.8 Hz, 1H, C3−H), 5.12 (t, J = 9.8 Hz, 1H, C4−H), 5.00 (dd, J = 3.7 and 9.8 Hz, 1H, C2−H), 4.19−4.39 (m, 3H, C5−H and CH_2), 2.01 (s, 3H, CH_3), 1.99 (s, 3H, CH_3), 1.98 (s, 3H, CH_3). ^{13}C NMR (63 MHz, $CDCl_3$) δ/ppm 170.03 (C═O), 169.74 (C═O), 169.32 (C═O), 160.62 (*C*═N), 150.37 (d, 2C), 129.80 (4C), 125.48 (2C), 120.09 (t, 4C), 92.67 (C1), 90.63 (CCl_3), 70.48 (d, 1C), 69.78, 69.58, 67.80, 66.31 (d, 1C), 20.66 (CH_3), 20.56 (CH_3), 20.40 (CH_3). ^{31}P NMR (101 MHz, $CDCl_3$) δ/ppm −11.65. TOF MS (ES^+) 704 (M + Na^+). HR−MS (ES^+) calculated for $C_{26}H_{27}Cl_3NO_{12}P$ + Na^+, 704.0234; found, 704.0240.

2,3,4-Tri-*O*-acetyl-β-D-glucose-6-diphenylphosphate-1-phosphate Triethylamine Salt.[51] To a mixture of 2,3,4-tri-*O*-acetyl-α-D-glucose-6-diphenylphosphate-1-trichloroaetimidate (100 mg, 0.147 mmol) in dry dichloromethane (40 mL) was added 72 μL of H_3PO_4 in THF solution (1.12 g of H_3PO_4 (88%) in 5 mL of THF, dried over $MgSO_4$). After the mixture was stirred at room temperature for 45 min, triethylamine (1 mL) was added, and the mixture was concentrated to dryness in vacuo under 25 °C. The resulting solid product was washed with acetone (5 mL × 3) and dried in vacuo. ^{1}H NMR (250 MHz, $CDCl_3$) δ/ppm 7.43 (m, 4H, Ar−H), 7.21−7.35 (m, 6H, Ar−H), 5.27 (t, J = 9.5 Hz, 1H, C1−H), 5.13 (t, J = 8.2 Hz, 1H), 4.93 (dd, J = 10.1 Hz and 9.7 MHz, 1H), 4.77 (dd, J = 7.9 and 9.5 Hz, 1H), 4.61 (m, 1H), 4.46 (m, 1H), 4.02 (dd, J = 2.1 Hz and 9.9 Hz, 1H), 3.15 (q, J = 7.3 Hz, 6H, $3CH_3CH_2$), 2.10 (s, 3H, CH_3), 1.98 (s, 3H, CH_3), 1.94 (s, 3H, CH_3), 1.23 (t, J = 7.3.Hz, 9H, $3CH_3CH_2$). ^{31}P NMR (101 MHz, $CDCl_3$) δ/ppm 2.93, −10.71. Calculated for $C_{30}H_{43}NO_{15}P_2$ 719. TOF MS (ES^+) found 720 (M + H^+). This product was used for the next step without further purification.

β-D-Glucose-1,6-diphosphate.[85] The crude 2,3,4-tri-*O*-acetyl-β-D-glucose-6-diphenylphosphate-1-phosphate triethylamine salt was dissolved in 10 mL of methanol, and the solution was then passed through a IR-120 (H^+) column, and the column was washed with methanol. The volume of combined methanol solution was about 40 mL. PtO_2 (10 mg) was added to this solution, and the mixture was stirred at room temperature and at atmospheric pressure with pure hydrogen for 24 h. After the mixture was filtered, triethylamine (2 mL) was added, and then the mixture was concentrated under reduced pressure. To the resulting solid product was added a fresh solution of CH_3ONa (100 mg) in methanol (5 mL). The mixture was stirred at room temperature for 15 h and was concentrated in vacuo. Water (5 mL) was added, and the inorganic phosphate was then precipitated by adding an excess of aqueous magnesium chloride solution. The solution was filtered, and the filtrate was passed through a IR-120 (H^+) column. After neutralization (pH 7) with saturated $Ba(OH)_2$ solution, the volume of the solution was concentrated to about 2 mL. When the solution was heated, barium salt of β-D-glucose-1,6-diphosphate was precipitated and was separated by filtration, and washed with hot water, ethyl alcohol, and ether.

The barium salt was converted to the sodium salt by dissolving in a large amount of cold water, and the water solution was passed through a IR-120 (Na^+) column, then lyophilized to give 40 mg of a white solid, 64%. ^{1}H NMR (500 MHz, D_2O) δ/ppm 4.81 (t, J =

(82) Lardy, H. A.; Fischer, H. O. L. *Biochem. Prep.* **1952**, *2*, 39–44.
(83) Chittenden, G. J. F. *Carbohydr. Res.* **1988**, *183*, 140–143.
(84) Wang, J.; Li, J.; Tuttle, D.; Takemoto, J. Y.; Chang, C. W. T. *Org. Lett.* **2002**, *4*, 3997–4000.
(85) Posternak, T. *J. Biol. Chem.* **1949**, *180*, 1269–78.

7.8 Hz, 1H, C1−H), 4.01 (dd, J = 6.0 and 11.7 Hz, 1H, C6−H), 3.91−3.95 (m, 1H, C6−H′), 3.43−3.48 (m, 3H, C5/4/3-H), 3.25 (t, J = 7.8 Hz, 1H, C2−H). ^{13}C NMR (63 MHz, D_2O) δ/ppm 97.45 (d, J = 4.8 Hz, C1), 75.43 (d, J = 6.7 Hz, C5), 75.15 (C3), 74.23 (d, J = 6.7 Hz, C2), 69.05 (C4), 63.60 (d, J = 4.3 Hz, C6). ^{31}P NMR (101 MHz, D_2O) δ/ppm 2.21, 0.64. TOF MS (ES^-) 361 ($M - 3Na^+ + 2H$), 339 ($M - 4Na^+ + 3H$). HR−MS (ES^-) calculated for $C_6H_{13}O_{12}P_2^-$, 338.9882; found, 338.9867.

The concentrations of stock solutions of βG16BP used for kinetic studies were calibrated by ^{1}H NMR using 1 mM TSP as an internal integration standard.

Expression and Purification of βPGM. βPGM was expressed in *E. coli* BL21(DE3) and purified by published procedures.[45] Despite not being phosphorylated in our hands,[45] βPGM showed some activity in the absence of any added G16BP. We established that the commercial βG1P did not contain detectable concentrations (by ^{1}H, ^{31}P, and ^{13}C NMR spectroscopy) of bisphosphate as a contaminant[5,49] (that could act as a reaction activator in catalytic amounts).

Enzyme concentrations were measured using $\varepsilon_{280} = 20.6$ cm^{-1} μM^{-1} cm^{-1} determined by the Biuret method[86] with commercial BSA standards (Sigma) used for the calibration. Burst amplitudes in presteady-state kinetics corresponded to the protein concentrations obtained by the Biuret method.

Kinetic Measurements. Coupled Assays for βPGM Kinetic Measurements. The most frequently used assay for phosphoglucomutase kinetic studies is the glucose-6-phosphate dehydrogenase (G6PDH) coupled assay.[87] The direct product of the βPGM-catalyzed reaction is the β-anomer of G6P, which spontaneously equilibrates with αG6P in solution until the equilibrium between both anomers is reached (K_{eq} = 1.4).[87−89] Because G6PDH's original substrate is βG6P,[47] it is not expected that the apparent rate of βPGM reaction will be limited by the rate of anomerization as can occur with αPGM[87] (under conditions of excess G6PDH and NAD^+). Fluoride does not inhibit the activity of the coupled enzyme up to 100 mM concentrations.

For the hydrolase reactivity of βPGM, a glucose dehydrogenase coupled assay (GDH) as described by Zhang et al.[7] was used. Again, at the concentration used, fluoride does not have any effect on GDH activity.

Fluoride Binding and Inhibition Experiments under Crystallization Conditions. i. Mutase Reaction. A stock mixture containing βPGM (0.22 mM), βG1P (6 mM), and $MgCl_2$ (10 mM) in buffer (50 mM HEPES, pH 7.2) was incubated at room temperature in test tubes with no fluoride and with 100 mM NH_4F. The mutase reaction was initiated by the addition of 100 μL (75 mM) of substrate, and the final total volume of the reaction mixture was 1250 μL. Aliquots (200 μL) were taken at fixed time intervals, and the reaction was stopped by heat denaturation (100 °C, in the Eppendorf thermoblock). Denaturated protein was removed by centrifugation, and the concentration of G6P was determined in the supernatants spectrophotometrically using the G6PDH assay described above.

ii. Hydrolase Reaction. The stock solution mixture containing βPGM (0.46 mM), G6P (1 mM), and $MgCl_2$ (10 mM) in buffer (50 mM HEPES, pH 7.2) was incubated at room temperature in test tubes without fluoride and with NH_4F (final concentration 100 mM) for a fixed time (15 min). The hydrolase reaction was started by addition of G6P. Incubations of G6P with βPGM were filtered through a Vivaspin column (Sartorius) membrane with a 10 kDa cutoff. A small volume of the supernatant was removed, and the concentration of βPGM was determined spectrophotometrically (ε_{280} = 20.6 cm^{-1} μM^{-1}), but the reaction was stopped in the surplus supernatant volume, and concentrations of G6P in the supernatant and flow-through solutions were determined using the G6PDH coupled assay as described above.

Steady-State βPGM Kinetic Assays. All steady-state βPGM assays were carried out in a Molecular Devices Microtiterplate Spectramax Plus Reader at 25 °C in 50 mM buffer (HEPES, pH 7.2) with 100 μL total volume containing 2 mM $MgCl_2$ and 5 nM βPGM unless stated otherwise. The appearance of G6P and glucose was monitored in a coupled assays with G6PDH (obtained from Sigma, [G6PDH] = 5 U/mL; one unit U is defined as the amount of enzyme that generates 1 μmol product per minute; [NAD^+] = 0.5 mM) and GDH (obtained from Sigma, [GDH] = 20 U/mL; one unit U is defined as the amount of enzyme that generates 1 μmol product per minute; [NAD^+] = 0.5 mM), respectively, following the absorbance at 340 nm. Reactions were initiated by the addition of the substrate. The steady-state rates were calculated from the linear portions of time courses and when less than 20% of substrate was converted. Fluoride inhibition of G6PDH and GDH could not be detected below 100 mM in our experimental setup. Any inhibitory effects can therefore be ascribed to βPGM alone.

Presteady-State Assays. The presteady-state (burst) kinetics of βPGM with its true cofactor βG16BP were carried out in a stopped-flow apparatus (Applied Photophysics, SX.18MV). Reactions were initiated by mixing equal amounts of two buffer solutions of K^+ HEPES (50 mM) containing $MgCl_2$ (2 mM, pH 7.2) in a mixing chamber: one containing the enzyme and the other βG16BP, G6PDH, and NAD^+. The reaction product G6P was oxidized enzymatically by G6PDH, and its formation was followed spectrophotometrically at 340 nm by measuring NADH accumulation.

Data Analysis. The rate constants from the initial rate data obtained in the presence of βG16BP cofactor were analyzed according to eq 1, derived assuming a substrate-inhibited ping-pong mechanism, by modified nonlinear regression analysis[55] using a program originally written by Duggleby.[56] Equation 1 was fitted simultaneously to all measured initial rates at different βG1P (substrate) and βG16BP (cofactor) concentrations.

The progress curves obtained in the presence of αG16BP cofactor were analyzed using DynaFit software.[57] The DynaFit program (BioKin Ltd.) calculates and solves a system of differential equations that correspond to the time-dependent change in concentration of each species involved in a given reaction mechanism, including the products. A family of kinetic traces at varying substrate concentrations can be fitted globally to one or more kinetic models. The assignments of the different models tested were made according to general criteria for goodness of fit.

The individual progress curves obtained at different concentrations of magnesium and fluoride were analyzed according to eq 3.[60] The Hill and linear equations were fitted to the sum of the calculated parameters k_a and k_b versus fluoride and magnesium concentrations, respectively. Nonlinear regression (Kaleidagraph, Synergy Software) was used for fitting. The mathematical relations between Y_0, Y_1, Y_2, and (k_a+ k_b) (see Supporting Information) were used for the final calculation of individual kinetic parameters in Scheme 6.

Acknowledgment. M.G. thanks the EU for a Marie-Curie fellowship and LFO CONACYT for a doctoral fellowship. F.H. is an ERC Starting Investigator. This work was funded by the BBSRC. We acknowledge helpful discussions with Mike Blackburn and thank Tony Kirby for comments on the manuscript.

Supporting Information Available: Calculation of the number of molecules of βG16BP that can accumulate during the reaction; kinetic equations for steady- and presteady-state analyses; NMR analysis of the stereochemistry of the βG16BP cofactor; and kinetic data for reaction of βG1P with βPGM in the absence of added cofactor. This material is available free of charge via the Internet at http://pubs.acs.org.

JA806421F

(86) Price, N. C. In *Enzymology Labfax*; Engel, P. C., Ed.; Academic Press: New York, 1996; pp 34−41.
(87) Ray, W. J.; Peck, E. J. *Enzymes*, 3rd ed.; Academic Press: New York, 1972; Vol. 6, pp 407−477.
(88) Salas, M.; Vinuela, E.; Sols, A. *J. Biol. Chem.* **1965**, *240*, 561–8.
(89) Balaban, R. S.; Ferretti, J. A. *Proc. Natl. Acad. Sci. U.S.A.* **1983**, *80*, 1241–5.